Published in final edited form as:
Wiley Interdiscip Rev Nanomed Nanobiotechnol. 2012 ; 4(5): 492–510. doi:10.1002/wnan.1176.

PHASE-SHIFT, STIMULI-RESPONSIVE PERFLUOROCARBON NANODROPLETS FOR DRUG DELIVERY TO CANCER

Natalya Rapoport
Department of Bioengineering, University of Utah, 72 S. Central Campus Dr., Room 2750, Salt Lake City, UT 84112, USA, Tel: 801-231-2480, natasha.rapoport@utah.edu

Abstract

This review focuses on phase-shift perfluorocarbon nanoemulsions whose action depends on an ultrasound-triggered phase shift from a liquid to gas state. For drug-loaded perfluorocarbon nanoemulsions, microbubbles are formed under the action of tumor-directed ultrasound and drug is released locally into tumor volume in this process. This review covers in detail mechanisms involved in the droplet-to-bubble transition as well as mechanisms of ultrasound-mediated drug delivery.

Keywords

drug delivery; perfluorocarbon nanoemulsions; therapeutic ultrasound; acoustic droplet vaporization; droplet-to-bubble transition

During the last decade, nanoparticles have attracted special attention as drug carriers with multiple functionalities. The family of nanoparticles includes polymeric micelles, liposomes, hollow particles, nano- or microemulsion droplets, as well as metallic nanospheres, rods, shells and cages, and carbon based nanotubes and balls. Among various suggested drug carriers, three types, namely liposomes, polymeric micelles, and emulsions are the most extensively studied and developed drug carriers. These are spherical nanoparticles with a core-shell structure. Liposomes have aqueous internal compartment sequestered by a phospholipid shell, which allows encapsulation of water-soluble drugs in the inner core. Polymeric micelles are characterized by hydrophobic cores and hydrophilic shells; hydrophobic micelle cores serve as reservoirs of lipophilic drugs. Polymeric micelles are formed by amphiphilic block copolymers composed of hydrophobic and hydrophilic blocks; each block copolymer molecule spans both a core and a shell of a micelle. Emulsions are the oldest drug carriers that have been used in clinical practice for decades; in emulsions, oil droplets are stabilized by ionic or non-ionic surfactants or surfactant mixtures; in contrast to polymeric micelles, oil droplets in emulsion form a separate phase and are usually substantially larger than micelle cores. Size of emulsion droplets may be reduced to a nanoscale by the application of external energy and selection of appropriate surfactants and co-surfactants. Nanoemulsions formed by perfluorocarbon compounds present the main topic of the current review.

Drug encapsulation in nanocarriers including nanoemulsions may dramatically increase the effective aqueous solubility of highly potent drugs whose application has been hampered by low solubility. Encapsulation also prevents drug degradation under the action of body fluids and allows drug transport towards desired targets thus reducing side effects. Even highly

Correspondence to: Natalya Rapoport.

toxic and unstable cytolytic peptide melittin was effectively targeted to murine tumors after being incorporated into the lipid membranes of perfluorocarbon nanodroplets; effective tumor regression without substantial systemic toxicity was observed [1, 2]. The effectiveness of tumor targeting may be substantially enhanced by ligand/receptor interaction. This approach has been used to target perfluorocarbon nanodroplets to neovasculature and/or tumor cells by conjugating or incorporating ligands to $\alpha_v\beta_3$ integrins that are over expressed on the neo-endothelial vasculature, tumor cells, or inflamed tissues (see e.g. [3–5]).

Various chemotherapeutic drugs, imaging agents, and targeting moieties may be encapsulated in the same “teragnostic” nanocontainer. The ability to combine chemotherapeutic and imaging agents is especially important for energy-related processes such as ultrasound-mediated drug delivery because contrast-enhanced imaging can provide for precise energy deposition, early assessment of response to treatment, and allow personalized therapy [6–10].

The EPR effect as a basis of a passive tumor targeting of nanoparticles

Tumor tissue is characterized by poor vascularization, poorly organized vascular architecture, irregular blood flow and reduced lymphatic drainage. Leaky blood vessels and the lack of a lymphatic system result in an increased interstitial fluid pressure, which hinders convectional transport of drug carriers across blood vessel walls. Nevertheless, nanoparticles of appropriate size may accumulate in tumor tissue via the enhanced permeability and retention (EPR) effect [11] based on defective tumor microvasculature. A characteristic pore cutoff size range between 380 and 780 nm has been shown in a variety of tumors although in some tumors the size may increase up to 2 μm. This allows extravasation of drug-loaded nanoparticles through large inter-endothelial gaps [11–13], while the poor lymphatic drainage of tumors results in longer retention of extravasated particles in tumor tissue. In contrast to tumors, blood vessels in normal tissues have tight inter-endothelial junctions (characteristic cutoff size of 7.5 nm) which do not allow extravasation of nanoparticles. However, tumors demonstrate spatial heterogeneity in the distribution of inter-endothelial gaps, which results in a focal distribution of delivered nanoparticles [12]. This may have negative implications for the outcome of tumor nanotherapy.

Effective tumor accumulation of nanoparticles via the EPR effect requires sufficient particle residence time in circulation. To provide for this, nanoparticles are commonly coated with poly(ethylene oxide) (PEG) chains that decrease blood protein adsorption and particle recognition by the cells of the reticulo-endothelial system.

For effective therapeutic action, drugs should be released from carriers at the site of action. This can be provided by developing stimuli responsive drug carriers that release their drug load only in response to environmental or physical stimuli, such as pH, hyperthermia, light, or ultrasound; for recent reviews, see refs. [14, 15]. The state of the art in the application of ultrasound for targeted drug delivery is discussed below, with special emphasis on the role of triggered phase-shift transition inside of injected nanoparticles.

Ultrasound as a drug delivery modality offers a number of important advantages over other physical modalities. Ultrasound is the most cost effective, accessible, and does not use ionizing radiation (in contrast to CT/PET). Ultrasound imaging may be combined with ultrasound-mediated drug delivery using ultrasound-responsive nanoparticles. Ultrasound can be directed toward deeply located body sites, and tumor sonication with millimeter precision is feasible. Sonication may be performed non-invasively or minimally invasively through intraluminal, laparoscopic or percutaneous means. For extracorporeal sonication, the transducer is placed in contact with a water-based gel or a water layer on the skin, and no insertion or surgery is required.

Ultrasound-mediated drug delivery: mechanisms

Several mechanisms of ultrasound action in drug delivery applications have been discussed [16–20]; both ultrasound-triggered localized drug release from carriers and biological effects of ultrasound should be considered.

Thermal effects

Localized heating of tissues has been produced by various external stimuli, including ultrasound. In general, the heat produced depends on the tissue absorption of the energy and the rates of thermal diffusion and convection. Absorption of ultrasound is frequency dependent and increases monotonically with frequency. Note that even a moderate temperature increase may have serious biological consequences, e.g. significantly increase permeability of blood capillaries [21–23] or lead to cell membrane fluidization [24, 25]. These effects may be accompanied by mechanical permeabilization (poration) of cell membranes.

Thermal effects of ultrasound have been used with temperature sensitive liposomes that rapidly release their contents at physiologically tolerated tissue temperatures [22, 26–34]. Heating produces a gel-to-fluid phase transition in the phospholipid membrane that enhances diffusion and releases drug in the target region. These nanoparticles, loaded with the chemotherapeutic doxorubicin have been commercialized (ThermoDox®, Celsion Corp.), and are undergoing clinical trials in combination with RF thermal ablation [28, 35]. Ultrasound as a heating modality is also being studied for release of drugs from these and similar low temperature-sensitive liposomes [17, 32, 36–38]. In fact, liposomes remain the most broadly investigated ultrasound-responsive drug delivery vehicles.

Mechanical action of ultrasound: cavitation

This action can be substantially enhanced by the introduction of gas-filled microbubbles. In current clinical practice, microbubbles have been used as ultrasound contrast agents for cardiovascular imaging [39, 40] and for molecular imaging; see the review by Klibanov and references therein [41]. During the last decade, microbubbles have attracted attention as drug carriers and enhancers of drug and gene delivery. Several research groups have concentrated their efforts on developing microbubble-based drug delivery systems [18, 42–66].

In the ultrasound field, microbubbles grow and collapse in a process called inertial cavitation. Inertial cavitation of microbubbles creates microjets and shock waves that can create holes in blood vessels and cell membranes thus increasing their permeability for drugs, genes, and their carriers. The ultrasound-induced creation of pores in cell membranes is called sonoporation [17, 67–78].

At ultrasound energies that don’t induce inertial cavitation, microbubbles stably oscillate in the ultrasound field; this process is called stable cavitation. Stable cavitation of systemically injected microbubbles can induce alternating invagination and distention of blood vessel walls, which in turn can cause damage of the endothelial lining and temporarily increase blood vessel permeability [79–82]. For blood vessels that are large in comparison to microbubble sizes, invagination appears to be a major vessel damaging factor; for small blood capillaries, both invagination and distension result in endothelial damaging and increased permeability [80].

Ultrasound-induced cavitation has been used for opening liposomal membranes [19, 83, 84]. The development of ultrasound-responsive stable liposomes that manifest prolonged circulation time and effective tumor targeting has been recently reported [85–87]. Ultrasound also manifests a potential to affect the intracellular drug distribution by overcoming the barrier created by the nuclear membrane [88].

Drug-loaded microbubbles would be attractive ultrasound-responsive drug carriers. This approach may be very beneficial for drug targeting to intravascular targets [83, 84, 89–103]. However, the currently used contrast agents present a number of inherent problems as *tumor-targeted* drug carriers. The ideal ultrasound-mediated tumor-targeted drug carrier should satisfy a number of requirements: stability in circulation; drug retention until activated; size that allows extravasation through defective tumor vasculature; ultrasound responsiveness. The very short circulation time (minutes) of commercially available microbubbles and their relatively large size (two to ten micrometers) do not allow effective extravasation into tumor tissue, thus preventing effective drug targeting. Only a fraction of the drug ultrasonically released from microbubbles into circulation is expected to reach tumor tissue while other drug will circulate with blood flow and eventually reach off-target sites. However the unexpectedly efficient therapeutic action of microbubbles combined with low duty cycle ultrasound on subcutaneously grown glioma xenografts was recently reported [104].

Mechanical action of ultrasound in the absence of cavitation

The most frequently discussed non-thermal and non-cavitation mechanisms are related to acoustic streaming and ultrasound radiation forces. Sound propagating through a medium produces a force upon the medium, resulting in translation of the fluid, called acoustic streaming, and also on particles suspended in the medium, called the radiation force [44, 45]. Acoustic streaming and the radiation force each produce particle translation in the acoustic field and their effects may be combined. It has been demonstrated that acoustic streaming and/or radiation force presents a means to localize and concentrate droplets and bubbles near a vessel wall, which may assist the delivery of targeted agents. The application of radiation force pulses can bring the delivery vehicle into proximity with the cell for successful adhesion of the vehicle or its fragments to cell membranes [105]. Actively targeted acoustically active lipospheres were used to deliver paclitaxel (PAX) to HUVEC cells overexpressing $\alpha_v\beta_3$ integrins [106]. Circulating particles were deflected by radiation force to a vessel wall and could subsequently be fragmented by stronger pulses. Drug delivery was limited to the focal area of ultrasound [44]. A similar strategy was used for enhancing the cellular interaction of targeted lipid-coated perfluorooctylbromide (PFOB) nanoparticles with melanoma cells [107]. Ultrasound (2 MHz at 1.9 mechanical index) applied in conjunction with PFOB nanodroplets (both non-targeted and targeted) elicited no changes in the cell survival, monolayer permeability or transendothelial electrical resistance and did not disrupt cell monolayers. The authors hypothesized that ultrasound facilitated drug transport from the perfluorocarbon nanoparticles into cells by direct cell/nanoparticle interaction that stimulated lipid exchange and drug delivery rather than by cavitation-induced effects on cell membranes.

The frequency dependence of particle velocity is different for acoustic streaming and radiation force, which allowed for the discrimination of the role of each factor in translation of perfluorocarbon nanodroplets in the ultrasound field in Dayton et al.[45]. Experimental results obtained in this paper led the authors to conclude that acoustic streaming dominated in large blood vessels (with a magnitude of hundreds of micrometers per second for particle displacement). Radiation force on the particles was expected to dominate in the microvasculature because acoustic streaming decreases with decreasing vessel diameter.

The mismatch between acoustic impedances of water or tissue (1.4 MRayl) and perfluorocarbon (apprx. 0.3 MRayl) may promote generation of sheer stresses in the presence of microbubbles. Sheer stresses may increase inter-endothelial gaps and extra-cellular space, resulting in increased extravasation and diffusion of drug carriers and drugs in sonicated tissues [108–114]. Acoustic streaming and radiation force can also push nanoparticles through blood capillary walls thus enhancing extravasation of drug carriers or

macromolecular drugs [18, 44, 45, 115, 116]. In an interesting novel application, the ultrasound radiation force was used to modulate ligand exposure on the surface of targeted contrast agents [117]. In the initial nanoparticle, the ligand had been hidden in the droplet shell; under the action of ultrasound, the ligand was exposed to the cell receptor and the properties of the contrast agent surface changed from stealth to sticky.

Ultimately, the thermal and mechanical action of ultrasound on drug carriers and biological tissues enhance perfusion, increase extravasation of drugs and/or carriers, and enhance drug diffusion throughout tumor tissue, facilitating drug penetration through various biological barriers. The increased intracellular uptake of nanoparticles, genes, and drugs results in significantly enhanced therapeutic efficacy of conventional drugs [52, 118–124].

Ultrasound as a component of drug delivery system may be coupled with a variety of drug carriers. Local drug release may be activated using carriers that are sensitive to mechanical, thermal, or both factors [18, 45, 46, 55, 63, 64, 85, 125–131]. Ultrasound treatment has also been associated with an induced immune response to tumors [132–135].

Ultrasound-Responsive Phase-Shift Nanoemulsions

The use of microbubbles as drug carriers is very attractive because it can allow combining cost-effective ultrasound imaging with ultrasound-mediated therapy. Due to high acoustic impedance, both PFP droplets (~0.3 MRayl) and bubbles ($\ll$0.3 MRayl) manifest echogenic properties [136]; however bubbles manifest much higher echogenicity than droplets, which creates better contrast in ultrasound images. Even more importantly, only bubbles undergo inertial cavitation (growth and collapse of bubbles in an ultrasound field), which concentrates ultrasound energy and substantially enhances ultrasound-mediated drug delivery. Though drug delivery from micelles, liposomes, or emulsions may be ultrasonically enhanced even without microbubbles [14, 45, 129, 130, 137, 138], presence of microbubbles dramatically increases intracellular uptake of drugs or genes [56, 83, 139, 140].

Several research groups have concentrated their efforts on developing microbubble-based drug delivery systems [18, 46, 62, 63, 83, 131, 141, 142]. However, as mentioned above, these systems present inherent problems for tumor targeting. Their very short circulation time (minutes) and micrometer-range size do not allow effective extravasation into tumor tissue, which is an essential prerequisite for effective tumor targeting.

The way to solve the above problem may consist in developing stable, drug-loaded, nano-scaled microbubble precursors that would effectively accumulate in tumor tissue by passive or active targeting and then convert into microbubbles *in situ* under the action of tumor-directed ultrasound. With this in mind, Utah team has recently developed amphiphilic block copolymer stabilized echogenic (i.e. ultrasound contrast generating) perfluorocarbon (PFC) nanoemulsions that converted into microbubbles under ultrasound irradiation [56, 122, 123, 143, 144]. The nanoemulsions (droplet size range from 200 nm to 750 nm depending on the type of the copolymer and perfluorocarbon to copolymer concentration ratio) were produced from drug-loaded poly(ethylene oxide)-co-poly(L-lactide) (PEG-PLLA), poly(ethylene oxide)-co-poly(D,L-lactide) (PEG-PDLA), or poly(ethylene oxide-co-polycaprolactone (PEG-PCL) micelles. Their important properties combine drug carrying, tumor-targeting, enhancing intracellular drug delivery, and enhancing the ultrasound contrast of tumors.

In what follows, we will focus on perfluorocarbon nanoemulsions that can release their drug load in response to the ultrasound-induced phase shift.

Droplet-to-bubble phase transition in dodecafluoropentane nanoemulsions

It has been known for more than a decade starting with a pioneering work by Apfel that specially designed perfluorocarbon droplets can convert into microbubbles under the action of ultrasound irradiation [145]. This effect, called acoustic droplet vaporization, or ADV has been thoroughly investigated for albumin coated micrometer-sized dodecafluoropentane (DDFP) droplets in the works of the University of Michigan group [136, 146–156]. Acoustic droplet vaporization was tested for temporal and spatial control of tissue occlusion [149], as cavitation nucleation agents for non-thermal ultrasound therapy [155, 157], for enhancing gene transfer, and for phase aberration correction [148].

Kripfgans *et al.*[136] observed that micrometer-sized PFP droplets can be vaporized into gas bubbles with the application of short tone bursts in the diagnostic frequency range (1.5–8 MHz). The resulting bubbles were 20–80 μm in diameter. The threshold for vaporization decreased with increasing ultrasound frequency and insonation time and by introducing microbubbles [136, 151]. The vaporization threshold was higher for smaller droplets [147]. These experiments were recently complemented with optical imaging of the droplet-to-bubble transition using the ultra-high speed imaging camera [158].

In the works by Rapoport *et al.*, droplet-to-bubble transition in DDFP droplets was shown to be catalyzed by pre-existing droplets; DDFP droplets were inserted into the gel matrix. The observed catalytic effect was stronger for lower ultrasound frequencies (Figure 1) [124, 144]. The core of nanodroplets used in the above studies was formed by DDFP that has a boiling temperature of 29 °C at atmospheric pressure and therefore manifests high propensity for vaporization at heating. However, for small droplets stabilized by elastic copolymer shells, the Laplace pressure (i.e. the pressure difference between the inside and the outside of droplet) may substantially increase boiling temperature. This effect is caused by the surface tension at the interface between droplet and bulk liquid.

The Laplace pressure is given by

$$\Delta P = P_{inside} - P_{outside} = \frac{2\sigma}{r} \quad (1)$$

where P_{inside} is the pressure inside a droplet, P_{outside} is the pressure outside a droplet, σ is the surface tension, and r is droplet radius.

Excessive pressure inside a droplet results in increase of DDFP boiling temperature. This phenomenon has important consequence for drug delivery. Because Laplace pressure is inversely proportional to droplet size according to eq.1, smaller droplets have higher boiling temperatures than larger droplets. The surface tension at the DDFP/water interface for “naked” (i.e. not surfactant coated) DDFP droplets is 56 ± 1 mN/m.

Using the known parameters of the Antoine equation for the pressure dependence of the DDFP vaporization temperature [159], the dependence of the DDFP droplet vaporization temperature on droplet size presented in Figure 2 [144] was calculated for two values of the interfacial tension, 30 mN/m and 50 mN/m, that are typical for PEG-coated colloid particles [160].

As indicated by Figure 2, even for low values of the surface tension, droplets smaller than 4 μm will remain in the liquid state at physiological temperatures while larger droplets will evaporate. However, droplets of these sizes are not present in initial nanoemulsions. Therefore nanodroplets would be expected to circulate as liquid droplets, which is beneficial for their extravasation into tumor tissue. However temperature increase is not the only factor that may induce droplet-to-bubble transition. Other factors include nanoemulsion injections

through small diameter needles and ultrasound (i.e. ADV) [124, 144]. The droplet-to-bubble transition upon injection through needles was first observed for the Echogen microemulsions; its clinical implications have been discussed in ref. [39]. Upon nanoemulsion injection, some generation of microbubbles in the vascular bed may be beneficial because microbubble/ultrasound/endothelial lining interaction may result in increased vascular permeability [79, 80, 82, 116, 161–164]. However massive transition of drug-loaded PFP nanodroplets into microbubbles inside blood vessels should be prevented because only nanosized particles extravasate into tumor tissue. To prevent excessive droplet-to-bubble transition in vasculature, systemic injection of PFP nanoemulsions should be performed either by infusion or injection through low-gauge needles. On the other hand, after extravasation into tumor tissue, massive droplet-to-bubble transition may be very beneficial. The latter may be initiated by tumor sonication with therapeutic ultrasound.

DDFP bubbles observed after the vaporization of DDFP nanodroplets in refs. [123, 124, 136, 143, 144, 151] were undoubtedly secondary bubbles formed from primary bubbles. Ignoring secondary mechanisms, maximum increase of the droplet diameter upon complete DDFP vaporization cannot exceed a five-fold increase [47, 56, 136]. Therefore for a 500-nm diameter droplet, the expected bubble size upon complete vaporization would be 2.5 μm. However, bubbles of much larger sizes (tens and even hundreds micrometers) have been observed upon DDFP droplet vaporization. There are at least three different mechanisms of bubble growth: (1) transition of the preserved liquid into the gaseous phase inside a confined particle space resulting in a maximal 5-fold increase in droplet diameter as explained above; (2) droplet coalescence with bubbles or bubble coalescence between themselves; and (3) diffusion of dissolved air and/or DDFP from small bubbles into larger bubbles (i.e., Oswald ripening). Oswald ripening may play a significant role in gel or solid matrices where droplet and bubble diffusion and collisions are restricted or stalled.

The increase of bubble size upon ultrasound-induced vaporization was tested for the embolotherapy. Experiments performed on the externalized rabbit kidney using albumin-coated DDFP microdroplets with initial diameter less than 6 micrometers showed perfusion reduction of more than 70% following the ADV. The authors hypothesized that this effect may be sufficient for cell death and possible tumor treatment via ischemic necrosis. It was also suggested that radiofrequency ablation of tumors might also benefit from ADV due to reduced perfusion and heat loss. These experiments were later extended to externalized canine kidneys [154]. Substantial reduction of cortex perfusion was achieved in some cases.

To elucidate physical mechanisms behind acoustic vaporization of DDFP droplets, Fabiilli *et al.* studied the relationship between ADV and inertial cavitation (IC) thresholds by probing the effects of fluid properties (gas saturation, temperature, viscosity, and surface tension), and droplet and ultrasound parameters that are known to affect inertial cavitation [146]. In all of these experiments, the ADV threshold was lower than the inertial cavitation threshold, indicating that the droplet-to-bubble transition preceded inertial cavitation.

The aim of the recent experiments by Schad and Hynynen [165] was to simultaneously measure the thresholds for vaporization and inertial cavitation of lipid encapsulated DDFP droplets of a clinically relevant size. The dependence of these thresholds on droplet size and exposure duration was investigated at room temperature and 37 °C at acoustic frequencies in the therapeutic range of 0.578 MHz to 2.855 MHz; the mean sizes of the droplets varied from 1.19 μm to 5.77 μm. The vaporization threshold was found to decrease with increasing droplet size and ultrasound frequency. In contrast, the inertial cavitation threshold was not significantly dependent on the droplet size and increased with increasing sonication frequency. At 37 °C, all droplets vaporized without inertial cavitation. The authors

underlined that the results were obtained for insonation times of 10 ms or shorter and that longer insonation times may yield different results. These results do not rule out the role of inertial cavitation in promoting droplet vaporization.

Earlier, Gieseke and Hynynen [166] showed that the cavitation threshold pressure was linearly dependent on the frequency (0.74–3.30 MHz) and not strongly dependent on the burst lengths of 20, 50 or 100 ms. Later Lo *et al.* [151] measured the dependence of the cavitation threshold on the pulse duration for micrometer-sized albumin-coated DDFP droplets at the pulse duration range from 20 μs to 20 ms at 1.44 MHz; cavitation threshold was found to be significantly increased for shorter pulses in this pulse duration range.

Furthermore, Gieseke and Hynynen [166] measured the inertial cavitation threshold for micrometer sized albumin-shelled droplets containing various PFC cores including those with higher boiling temperature than that of DDPF (i.e. perfluorohexane and perfluoromethylcyclohexane). The authors found that inertial cavitation thresholds did not noticeably depend on the perfluorocarbon molecular weights and boiling temperatures and, thus, the droplets did not need to be in a superheated state to be cavitated by ultrasound bursts. This was later confirmed in experiments with nano-sized perfluoro-15-crown-5-ether (PFCE) droplets that effectively converted into bubbles at ultrasound pressures that were only slightly higher than those for DDFP nanodroplets [123]. However the mechanism of bubble formation from nanodroplets with high boiling temperature is most probably fundamentally different from the droplet vaporization (see below).

Kawabata *et al.* [167] showed that nanometer-sized droplets containing a mixture of perfluoropentane (DDFP) and 2H,3H-perfluoropentane can be vaporized at diagnostic ultrasound frequencies (4 MHz - to 7.8 MHz) and that vaporization threshold could be changed by altering relative concentrations of the two PFCs in the droplet [168]. The authors hypothesized that the vaporization of a higher boiling temperature 2H,3H-perfluoropentane may have been caused not only to the directly delivered ultrasound energy but also by the energy deposited by ultrasonically induced bubbles of DDFP. “Catalysis” by the pre-existing microbubbles of the ultrasound-induced droplet-to-bubble transition of nanoscaled DDFP droplets inserted in the gel matrix was also observed by Rapoport *et al.* [124, 144], as illustrated above in Figure 1. This suggests that the droplet-to-bubble transition in nanoscaled droplets can be effectively catalyzed not only by mixing PFCs of various boiling temperatures but also by using a broad (or bimodal) size distribution of the initial PFC droplets because larger droplets conversion threshold is lower for larger droplets.

In vitro studies with a clinical high intensity focused ultrasound system showed a 2.5 times increase in temperature elevation when nanodroplets were present [169]. Similar results were later obtained by Rapoport *et al.*; droplet-to-bubble transitions and bubble oscillations in Agarose gels resulted in enhanced absorption of ultrasound energy and sample heating [123].

Droplet-to-bubble phase transitions in perfluoro-15-crown-5-ether nanoemulsions

Ultrasound-induced vaporization of perfluoro-15-crown-5-ether (PFCE) nanodroplets was studied by Rapoport *et al.* [123]. The PFCE has a boiling temperature of 146 °C at atmospheric pressure. However, initiating droplet-to-bubble transition in PFCE nanodroplets required only slightly higher ultrasound energies than those for DDFP [123] confirming the data by Gieseke and Hynynen [166]. The droplet-to-bubble transition in PFCE nanodroplets was induced by both, continuous wave or pulsed ultrasound [123] confirming that the droplet-to-bubble transition had a non-thermal mechanism. A possible mechanism of ultrasound-induced droplet-to-bubble transition in PFCE has been recently suggested by Rapoport *et al.* [123]. One possible factor involved in acoustically triggered droplet-to-bubble transition in PFC nanoemulsions is a high solubility of gases, particularly oxygen. This feature has

allowed using perfluorocarbon emulsions as blood substitutes [170]. According to Henry's law, the solubility of gases increases with pressure. It has been hypothesized that during the rarefactional phase of ultrasound, the evolution of dissolved oxygen into a gas phase occurred inside the nanodroplet shell, followed by rectified diffusion of dissolved gases from the surrounding liquid into the resulting nanobubble. According to this hypothesis, PFCE bubbles contain predominantly a mixture of oxygen and other ambient gases (as well as a low fraction of PFCE vapor in equilibrium with the PFCE liquid phase). The bubbles formed were transient in nature; when the ultrasound was turned off, equilibrium between nanodroplets and surrounding medium was restored and gases with super-equilibrium concentrations diffused out of bubbles, thus restoring PFCE nanodroplets that precipitated to the bottom of the test tube. The mechanism suggested has been corroborated by the fact that degassing PFCE nanoemulsions inhibited the droplet-to-bubble transition; the droplet-to-bubble transition was restored after the contact with air was re-established.

The mechanism of the bubble formation described above is different from true *vaporization* of droplets. However, independent of the specific mechanism of droplet-to-bubble transition, the effects associated with microbubble cavitation in the ultrasound field will be exerted on the nanodroplets and biological tissue.

Bubbles formed from either DDFP or PFCE nanodroplets were shown to oscillate and cavitate in the ultrasound field, as manifested by the generation of harmonic, sub-harmonic frequencies and broadband noise in the fast Fourier transform (FFT) spectra of the scattered ultrasound beam [123, 124, 143].

The material presented above implies that drug-loaded, nano-scaled droplets could serve as microbubble *precursors* that have a prospect of accumulating in tumors due to their nanoscale sizes and then convert into microbubbles *in situ* under tumor sonication.

Block copolymer stabilized perfluorocarbon nanoemulsions as drug carriers

Amphiphilic block copolymer stabilized PFC nanodroplets were used as drug carriers in works by Rapoport *et al.* [47, 56, 122–124, 143, 144]. To form block copolymer stabilized nanodroplets, perfluorocarbon (PFC) compounds, e.g. DDFP or perfluoro-15-crown-5-ether (PFCE) are introduced into micellar solutions of amphiphilic block copolymers (i.e. PEG-PDLA or PEG-PCL) and emulsified [47, 56, 123, 124]. At low PFC concentrations, PFC is dissolved in micelle cores. When the PFC concentration exceeds the limit of solubility in a micelle core, the PFC evolves into a separate nanodroplet phase so that former micelle core turns into a droplet shell; in some range of the PFC concentrations, micelles coexist with nanodroplets; at still higher PFC concentrations, all block copolymer is used for droplet stabilization and micelles disappear. The phase diagram of the PFC/copolymer system is presented schematically in Fig. 3 [47, 56, 123].

Droplet shells contain two layers: the inner layer formed by a hydrophobic block of a block copolymer (e.g. polylactide or polycaprolactone) and the outer layer formed by a hydrophilic block, usually PEG, as shown schematically in Figure 4A. If a lipophilic drug has been encapsulated in micelle cores, the drug is transferred from micelles onto the droplet surface and gets localized in the inner hydrophobic layer of the shell, as exemplified by the laser confocal imaging of doxorubicin (DOX) encapsulating droplets (Figure 4B).

An important advantage of phase-shift perfluorocarbon nanoemulsions as drug carriers is the ultrasound-induced generation of highly echogenic microbubbles as manifested by the formation of highly echogenic specks in ultrasound images [56, 123, 124, 143, 144];

perfluorocarbon nanodroplets are actually theragnostic agents that may allow monitoring nanodroplet-based therapy by ultrasound imaging.

Therapeutic outcomes and anticipated mechanisms of drug delivery with perfluorocarbon nanodroplets

In vitro, successful ultrasound-triggered delivery of paclitaxel (PTX) to monolayers of prostate cancer cells was reported by Dayton et al. for a phospholipid-coated perfluorohexane nanoemulsion developed by ImaRx [45]. Promising *in vitro* results were also obtained for delivery of a chemotherapeutic drug camptothecin to melanomas and ovarian cancer cells using ultrasound-activated perfluorocarbon nanodroplets stabilized by phospholipids and/or Pluronic F68 [5]. The formulations manifested a mean droplet diameter of 220–420 nm; confocal laser scanning microscopy confirmed nanoemulsion uptake into cells.

Fabiilli *et al.* tested *in vitro* albumin/soybean oil coated DDFP microdroplets as delivery vehicles for the lipophilic drug chlorambucil [152]. Application of ultrasound almost doubled cell killing by the drug.

Strong therapeutic effects using drug loaded perfluorocarbon nanoemulsions and ultrasound were also reported *in vivo*. Tumor treatment with drug-loaded lipid-stabilized PFOB or PFCE perfluorocarbon nanoemulsions was studied in works by the Lanza and Wickline group in the Washington University [1, 171–173]. The mechanism of ultrasound-mediated drug delivery proposed by the authors was based on the radiation force enhanced droplet/cell contact resulting in efficient drug delivery. According to this mechanism, ultrasound application enhances contact and fusion of cell membranes and phospholipid coated nanodroplets, resulting in the transfer of drug from nanodroplet shells into the interior of the cell. This mechanism can be operative for lipid-coated nanodroplets but would be hardly functioning for nanodroplets stabilized with PEG-containing block copolymers. The mechanism proposed by Rapoport *et al.* [124], for block copolymer stabilized perfluorocarbon nanodroplets is based on the droplet-to-bubble transition as presented schematically in Figure 5. Upon droplet-to-bubble transition, the particle volume increases dramatically, which is accompanied by a decrease of the thickness of the droplet shell. This is expected to favor the release of encapsulated drug, especially under the ultrasound action that “rips off” drug from the droplet surface. In addition, the increase of surface area decreases copolymer concentration on the surface and may even create “naked” patches that would also facilitate drug release.

Drug transition from bubbles to cells under the action of ultrasound was observed in model experiments presented in Fig. 6 [56]. DOX-loaded microbubbles were prepared by injections of drug-loaded nanodroplets into the capillary through the high-gauge needle (Figure 6A). Without ultrasound, breast cancer MDA MB231 cells incubated with microbubbles for 30 minutes did not develop visible fluorescence indicating the DOX was tightly retained in the microbubble shells. A 30-s exposure to 3-MHz ultrasound resulted in bubbles loosing fluorescence or being popped while cells acquired strong fluorescence (Figure 6B).

Drug retention by nanodroplets and microbubbles in vivo was confirmed in experiments with bi-lateral ovarian carcinoma tumors inoculated in a nude mouse were used (Figure 7). This mouse was treated by four systemic injections of nanodroplet encapsulated PTX (20 mg/kg as PTX) given twice weekly; only one (the right) tumor was sonicated by 1-MHz CW ultrasound at a nominal output power density 3.4 W/cm^2 with exposure duration of 1 min. The unsonicated left tumor grew with the same rate as control tumors. In contrast, the sonicated tumor appeared completely resolved after the treatments. This data suggested that

without ultrasound, the drug (paclitaxel) was tightly retained inside the DDFP droplet walls formed by a PEG-PLLA block copolymer, but was effectively released under the action of tumor-directed therapeutic ultrasound. Tight drug retention by the nanodroplet carrier *in vivo* is expected to provide protection for healthy tissues. On the other hand, effective ultrasound-induced PTX release into the tumor volume results in efficient localized tumor regression.

The therapeutic properties of drug-loaded DDFP and PFCE nanodroplets combined with 1-MHz ultrasound were reported by Rapoport *et al.* [123, 124]. The effects of the empty (i.e. not drug loaded) and PTX-loaded PFCE nanodroplets were compared in experiments with pancreatic tumor bearing mice. Tumors were transfected with red fluorescence protein (RFP) in order to allow intravital imaging. Cell survival monitoring was based on the fact that dead cells lose fluorescence. Tumors were sonicated using a focused ultrasound transducer under the MRI control with temperature monitored during treatment using MRI thermometry [123].

In this and similar experiments, no trace of tumor cell death was observed in mice injected with empty nanodroplets. In contrast, tumor cell death was clearly manifested in mice injected with PTX-loaded nanodroplets (Figure 8, compare tumor fluorescence images before (A) and after (B) focused ultrasound treatment). The dark area of non-viable cells (approximately 4 mm diameter “crater”) corresponded to the area treated with focused ultrasound. Despite the fact that only a fraction of the total tumor volume was treated by ultrasound, a significant delay of tumor growth was observed in a mouse treated with PTX-loaded nanoemulsions combined with focused ultrasound [123]. These and similar results suggest that: (i) the therapeutic action results from the action of drug rather than mechanical or thermal cell killing by ultrasound; (ii) the therapeutic action of nanodroplet-encapsulated drug is substantially enhanced by ultrasound whether this results from enhanced nanodroplet extravasation, ultrasound-triggered drug release from nanodroplets, hyperthermia effect caused by a 10 °C additional heating, enhanced intracellular droplet and drug uptake, or all of the above; (iii) the delayed tumor growth in the PTX-treated mouse suggests that under ultrasound, drug was spread from sonicated areas throughout the tumor volume by enhanced convection or diffusion. A strong therapeutic effect was also observed for a breast cancer treatment with PFCE nanodroplet-encapsulated PTX and focused ultrasound [123].

In the experiments by the Lanza and Wickline group, a technology was developed to impart active targeting properties to lipid coated nanodroplets. Integrin-targeted perfluorocarbon-based nanoparticles (250 nm diameter) were used for imaging $\alpha_v\beta(3)$ integrin receptor expression in tumors. The tumor-to-muscle droplet accumulation ratio was found to be 7 for targeted nanodroplets and 3 for non-targeted nanodroplets. Targeted nanodroplets were used for diagnosis and therapy of atherosclerosis [3, 174, 175]. This group also used molecularly targeted lipid-coated perfluorocarbon-based nanoparticles for *in vivo* delivery of a highly toxic amphipathic cytolytic peptide, melittin, to tumor bearing mice. Melittin was incorporated into the outer lipid monolayer of a perfluorocarbon nanoparticle. The authors observed a dramatic reduction in tumor growth without any apparent signs of toxicity. Furthermore, it was demonstrated that molecularly targeted nanocarriers selectively delivered melittin to multiple tumor targets, including endothelial and cancer cells, supposedly through a hemifusion mechanism. The review paper on using liquid perfluorocarbon nanoparticles as ^{19}F molecular imaging and targeted drug delivery agents in cancer and cardiovascular diseases has been recently published by this group [171].

For delivering water soluble compounds (fluorescein or thrombin), a double emulsion technique has been developed [153].

A step forward in enhancing contrast and delivery properties of perfluorocarbon nanodroplets has been recently made by Emelianov's group[176]. The authors manufactured so called photoacoustic nanodroplets by dispersing plasmonic nanoparticles in liquid perfluorocarbon nanodroplets as shown schematically in Figure 9. Pulsed laser irradiation triggered a liquid-to-gas phase transition in liquid perfluorocarbon droplet generating giant photoacoustic transients while the gaseous phase provided ultrasound contrast enhancement. It was demonstrated in phantom and animal studies that *via* optically triggered vaporization, photoacoustic nanodroplets acted as dual-contrast agents for both photoacoustic and ultrasound imaging (Figure 10).

A new approach to the generation of highly acoustically active prefluorocarbon droplet was recently suggested by Sheeran et al.[177]. The authors formulated droplets from a highly volatile decafluorobutane (DFB) (boiling point about -2 °C). The micrometer size droplets were generated from the condensed DFB gas by extrusion with a lipid formulation in HEPES buffer. The nanoscale droplets (200 nm to 300 nm diameter) were generated by condensation of preformed DFB microbubbles. Nanodroplets were stable at physiological temperatures but were activated by ultrasound using pressures within the FDA guidelines for diagnostic imaging, which may minimize the potential for bioeffects in humans. Acoustic characterization of submicrometer perfluorocarbon droplets studied by Reznik et al. also suggested that vaporization may be induced by diagnostic 7.5 MHz ultrasound at a mechanical index in diagnostic range (MI < 1)[178].

Taken together, these results suggest that drug loaded perfluorocarbon nanoemulsion in combination with ultrasound treatment can provide efficient therapy of a broad spectrum of diseases.

Conclusions and Outlook

Controlled drug delivery has been a goal of the bioengineering community ever since the 'magic bullet' concept was introduced by Paul Ehrlich over a century ago. By combining tissue targeting with active release mechanisms, this formerly illusive goal is turning into medical reality. An unprecedented opportunity to localize drug delivery is associated with developing stimulus responsive drug carriers, particularly ultrasound-responsive perfluorocarbon nanoemulsions. This novel technology has demonstrated excellent therapeutic potential in murine cancer models. Phase-shift nanoemulsions can be functionalized as actively targeted agents or as therapy-plus-imaging (theragnostic) probes.

Much *in vivo* work remains to be done for introducing phase-shift nanoparticles into clinical practice. Transition to experiments on larger animal models is a critical task. Passive targeting of nanoparticles may be more challenging in larger animals and human than in small animal models due to much smaller tumor-to-body volume ratio in large animals. Identifying more selective surface receptors is also a crucial task for active targeting. Design of optimal clinical drug delivery systems involves the identification of targets and tracking delivery systems in the body, guidance of therapy, and monitoring of immediate and delayed therapeutic response. These problems remain to be addressed in future translational studies.

Acknowledgments

The support by the NIH R01 EB1033 grant is greatly appreciated.

References

1. Soman NR, Baldwin SL, Hu G, Marsh JN, Lanza GM, Heuser JE, Arbeit JM, Wickline SA, Schlesinger PH. Molecularly targeted nanocarriers deliver the cytolytic peptide melittin specifically

to tumor cells in mice, reducing tumor growth. J Clin Invest. 2009; 119:2830–2842. [PubMed: 19726870]

2. Soman NR, Lanza GM, Heuser JM, Schlesinger PH, Wickline SA. Synthesis and characterization of stable fluorocarbon nanostructures as drug delivery vehicles for cytolytic peptides. Nano Lett. 2008; 8:1131–1136. [PubMed: 18302330]
3. Winter PM, Caruthers SD, Zhang H, Williams TA, Wickline SA, Lanza GM. Antiangiogenic synergism of integrin-targeted fumagillin nanoparticles and atorvastatin in atherosclerosis. JACC Cardiovasc Imaging. 2008; 1:624–634. [PubMed: 19356492]
4. Winter PM, Schmieder AH, Caruthers SD, Keene JL, Zhang H, Wickline SA, Lanza GM. Minute dosages of alpha(nu)beta3-targeted fumagillin nanoparticles impair Vx-2 tumor angiogenesis and development in rabbits. FASEB J. 2008; 22:2758–2767. [PubMed: 18362202]
5. Zhou HF, Chan HW, Wickline SA, Lanza GM, Pham CT. Alphavbeta3-targeted nanotherapy suppresses inflammatory arthritis in mice. FASEB J. 2009; 23:2978–2985. [PubMed: 19376816]
6. Lanza GM, Winter PM, Caruthers SD, Hughes MS, Hu G, Schmieder AH, Wickline SA. Theragnostics for tumor and plaque angiogenesis with perfluorocarbon nanoemulsions. Angiogenesis. 2010
7. Hahn MA, Singh AK, Sharma P, Brown SC, Moudgil BM. Nanoparticles as contrast agents for in-vivo bioimaging: current status and future perspectives. Anal Bioanal Chem. 2011; 399:3–27. [PubMed: 20924568]
8. Janib SM, Moses AS, MacKay JA. Imaging and drug delivery using theranostic nanoparticles. Adv Drug Deliv Rev. 2010; 62:1052–1063. [PubMed: 20709124]
9. Pan D, Lanza GM, Wickline SA, Caruthers SD. Nanomedicine: perspective and promises with ligand-directed molecular imaging. Eur J Radiol. 2009; 70:274–285. [PubMed: 19268515]
10. Pan D, Caruthers SD, Chen J, Winter PM, Senpan A, Schmieder AH, Wickline SA, Lanza GM. Nanomedicine strategies for molecular targets with MRI and optical imaging. Future Med Chem. 2010; 2:471–490. [PubMed: 20485473]
11. Iyer AK, Khaled G, Fang J, Maeda H. Exploiting the enhanced permeability and retention effect for tumor targeting. Drug Discov Today. 2006; 11:812–818. [PubMed: 16935749]
12. Campbell RB. Tumor physiology and delivery of nanopharmaceuticals. Anticancer Agents Med Chem. 2006; 6:503–512. [PubMed: 17100555]
13. Hobbs SK, Monsky WL, Yuan F, Roberts WG, Griffith L, Torchilin VP, Jain RK. Regulation of transport pathways in tumor vessels: role of tumor type and microenvironment. Proc Natl Acad Sci U S A. 1998; 95:4607–4612. [PubMed: 9539785]
14. Rapoport N. Physical stimuli-responsive polymeric micelles for anti-cancer drug delivery. Prog Polym Sci. 2007; 32:962–990.
15. MacEwan SR, Callahan DJ, Chilkoti A. Stimulus-responsive macromolecules and nanoparticles for cancer drug delivery. Nanomedicine (Lond). 2010; 5:793–806. [PubMed: 20662649]
16. Dalecki D. Mechanical bioeffects of ultrasound. Annu Rev Biomed Eng. 2004; 6:229–248. [PubMed: 15255769]
17. Deckers R, Moonen CT. Ultrasound triggered, image guided, local drug delivery. J Control Release. 2010
18. Ferrara KW. Driving delivery vehicles with ultrasound. Adv Drug Deliv Rev. 2008; 60:1097–1102. [PubMed: 18479775]
19. Frulio N, Trillaud H, Deckers R, Lepreux S, Moonen C, Quesson B. Influence of ultrasound induced cavitation on magnetic resonance imaging contrast in the rat liver in the presence of macromolecular contrast agent. Invest Radiol. 2010; 45:282–287. [PubMed: 20375844]
20. Miller MW, Miller DL, Brayman AA. A review of in vitro bioeffects of inertial ultrasonic cavitation from a mechanistic perspective. Ultrasound Med Biol. 1996; 22:1131–1154. [PubMed: 9123638]
21. Dreher MR, Liu W, Michelich CR, Dewhirst MW, Yuan F, Chilkoti A. Tumor vascular permeability, accumulation, and penetration of macromolecular drug carriers. J Natl Cancer Inst. 2006; 98:335–344. [PubMed: 16507830]
22. Kong G, Braun RD, Dewhirst MW. Hyperthermia enables tumor-specific nanoparticle delivery: effect of particle size. Cancer Res. 2000; 60:4440–4445. [PubMed: 10969790]

23. Kong G, Braun RD, Dewhirst MW. Characterization of the effect of hyperthermia on nanoparticle extravasation from tumor vasculature. Cancer Res. 2001; 61:3027–3032. [PubMed: 11306483]
24. Hayat H, Friedberg I. Heat-induced alterations in cell membrane permeability and cell inactivation of transformed mouse fibroblasts. Int J Hyperthermia. 1986; 2:369–378. [PubMed: 3805806]
25. Krupka T, Dremann D, Exner A. Time and dose dependence of pluronic bioactivity in hyperthermia-induced tumor cell death. Exp Biol Med (Maywood). 2009; 234:95–104. [PubMed: 18997100]
26. Dewhirst MW, Vujaskovic Z, Jones E, Thrall D. Re-setting the biologic rationale for thermal therapy. Int J Hyperthermia. 2005; 21:779–790. [PubMed: 16338861]
27. Gaber MH, Wu NZ, Hong K, Huang SK, Dewhirst MW, Papahadjopoulos D. Thermosensitive liposomes: extravasation and release of contents in tumor microvascular networks. Int J Radiat Oncol Biol Phys. 1996; 36:1177–1187. [PubMed: 8985041]
28. Hauck ML, LaRue SM, Petros WP, Poulson JM, Yu D, Spasojevic I, Pruitt AF, Klein A, Case B, Thrall DE, et al. Phase I trial of doxorubicin-containing low temperature sensitive liposomes in spontaneous canine tumors. Clin. Cancer Res. 2006; 12:4004–4010. [PubMed: 16818699]
29. Kong G, Anyarambhatla G, Petros WP, Braun RD, Colvin OM, Needham D, Dewhirst MW. Efficacy of liposomes and hyperthermia in a human tumor xenograft model: importance of triggered drug release. Cancer Res. 2000; 60:6950–6957. [PubMed: 11156395]
30. Kong G, Dewhirst MW. Hyperthermia and liposomes. Int J Hyperthermia. 1999; 15:345–370. [PubMed: 10519688]
31. Needham D, Anyarambhatla G, Kong G, Dewhirst MW. A new temperature-sensitive liposome for use with mild hyperthermia: characterization and testing in a human tumor xenograft model. Cancer Res. 2000; 60:1197–1201. [PubMed: 10728674]
32. Negussie AH, Yarmolenko PS, Partanen A, Ranjan A, Jacobs G, Woods D, Bryant H, Thomasson D, Dewhirst MW, Wood BJ, et al. Formulation and characterisation of magnetic resonance imageable thermally sensitive liposomes for use with magnetic resonance-guided high intensity focused ultrasound. Int J Hyperthermia. 2011; 27:140–155. [PubMed: 21314334]
33. Vujaskovic Z, Kim DW, Jones E, Lan L, McCall L, Dewhirst MW, Craciunescu O, Stauffer P, Liotcheva V, Betof A, et al. A phase I/II study of neoadjuvant liposomal doxorubicin, paclitaxel, and hyperthermia in locally advanced breast cancer. Int J Hyperthermia. 2010; 26:514–521. [PubMed: 20377362]
34. Yarmolenko PS, Zhao Y, Landon C, Spasojevic I, Yuan F, Needham D, Viglianti BL, Dewhirst MW. Comparative effects of thermosensitive doxorubicin-containing liposomes and hyperthermia in human and murine tumours. Int J Hyperthermia. 2010; 26:485–498. [PubMed: 20597627]
35. Poon RTP, Borys N. Lyso-thermosensitive liposomal doxorubicin: a novel approach to enhance efficacy of thermal ablation of liver cancer. Expert Opin Pharmacother. 2009; 10:333–343. [PubMed: 19236203]
36. Dromi S, Frenkel V, Luk A, Traughber B, Angstadt M, Bur M, Poff J, Xie J, Libutti SK, Li KC, et al. Pulsed-high intensity focused ultrasound and low temperature-sensitive liposomes for enhanced targeted drug delivery and antitumor effect. Clin Cancer Res. 2007; 13:2722–2727. [PubMed: 17473205]
37. Stone MJ, Frenkel V, Dromi S, Thomas P, Lewis RP, Li KC, Horne M 3rd, Wood BJ. Pulsed-high intensity focused ultrasound enhanced tPA mediated thrombolysis in a novel in vivo clot model, a pilot study. Thromb Res. 2007; 121:193–202. [PubMed: 17481699]
38. Staruch R, Chopra R, Hynynen K. Localised drug release using MRI-controlled focused ultrasound hyperthermia. Int J Hyperthermia. 2011; 27:156–171. [PubMed: 21158487]
39. Becher, H.; Burns, PN. Handbook for contrast echocardiograqphy. Frankfurt and New York: Springer Verlag; 2000.
40. Becher H, Lofiego C, Mitchell A, Timperley J. Current indications for contrast echocardiography imaging. Eur J Echocardiogr. 2005; 6(Suppl 2):S1–S5. [PubMed: 16360627]
41. Klibanov AL. Ultrasound molecular imaging with targeted microbubble contrast agents. J Nucl Cardiol. 2007; 14:876–884. [PubMed: 18022115]

42. Datta S, Coussios CC, Ammi AY, Mast TD, de Courten-Myers GM, Holland CK. Ultrasound-enhanced thrombolysis using Definity as a cavitation nucleation agent. Ultrasound Med Biol. 2008; 34:1421–1433. [PubMed: 18378380]
43. Datta S, Coussios CC, McAdory LE, Tan J, Porter T, De Courten-Myers G, Holland CK. Correlation of cavitation with ultrasound enhancement of thrombolysis. Ultrasound Med Biol. 2006; 32:1257–1267. [PubMed: 16875959]
44. Dayton P, Klibanov A, Brandenburger G, Ferrara K. Acoustic radiation force in vivo: a mechanism to assist targeting of microbubbles. Ultrasound Med Biol. 1999; 25:1195–1201. [PubMed: 10576262]
45. Dayton PA, Zhao S, Bloch SH, Schumann P, Penrose K, Matsunaga TO, Zutshi R, Doinikov A, Ferrara KW. Application of ultrasound to selectively localize nanodroplets for targeted imaging and therapy. Mol Imaging. 2006; 5:160–174. [PubMed: 16954031]
46. Ferrara K, Pollard R, Borden M. Ultrasound microbubble contrast agents: fundamentals and application to gene and drug delivery. Annu Rev Biomed Eng. 2007; 9:415–447. [PubMed: 17651012]
47. Gao Z, Kennedy AM, Christensen DA, Rapoport NY. Drug-loaded nano/microbubbles for combining ultrasonography and targeted chemotherapy. Ultrasonics. 2008; 48:260–270. [PubMed: 18096196]
48. Greenleaf WJ, Bolander ME, Sarkar G, Goldring MB, Greenleaf JF. Artificial cavitation nuclei significantly enhance acoustically induced cell transfection. Ultrasound Med Biol. 1998; 24:587–595. [PubMed: 9651968]
49. Hynynen K. Ultrasound for drug and gene delivery to the brain. Adv Drug Deliv Rev. 2008; 60:1209–1217. [PubMed: 18486271]
50. Kopechek JA, Abruzzo TM, Wang B, Chrzanowski SM, Smith DA, Kee PH, Huang S, Collier JH, McPherson DD, Holland CK. Ultrasound-mediated release of hydrophilic and lipophilic agents from echogenic liposomes. J Ultrasound Med. 2008; 27:1597–1606. [PubMed: 18946099]
51. Kost J, Mitragotri S, Gabbay RA, Pishko M, Langer R. Transdermal monitoring of glucose and other analytes using ultrasound. Nat Med. 2000; 6:347–350. [PubMed: 10700240]
52. McDannold N, Vykhodtseva N, Hynynen K. Effects of acoustic parameters and ultrasound contrast agent dose on focused-ultrasound induced blood-brain barrier disruption. Ultrasound Med Biol. 2008; 34:930–937. Epub 2008 Feb 2021. [PubMed: 18294757]
53. Miller DL, Averkiou MA, Brayman AA, Everbach EC, Holland CK, Wible JH Jr, Wu J. Bioeffects considerations for diagnostic ultrasound contrast agents. J Ultrasound Med. 2008; 27:611–632. quiz 633-616. [PubMed: 18359911]
54. Mitragotri S. Healing sound: the use of ultrasound in drug delivery and other therapeutic applications. Nat Rev Drug Discov. 2005; 4:255–260. [PubMed: 15738980]
55. Qin S, Caskey CF, Ferrara KW. Ultrasound contrast microbubbles in imaging and therapy: physical principles and engineering. Phys Med Biol. 2009; 54:R27–R57. [PubMed: 19229096]
56. Rapoport N, Gao Z, Kennedy A. Multifunctional nanoparticles for combining ultrasonic tumor imaging and targeted chemotherapy. J Natl Cancer Inst. 2007; 99:1095–1106. [PubMed: 17623798]
57. Shaw GJ, Meunier JM, Huang SL, Lindsell CJ, McPherson DD, Holland CK. Ultrasound-enhanced thrombolysis with tPA-loaded echogenic liposomes. Thromb Res. 2009; 124:306–310. [PubMed: 19217651]
58. Sheikov N, McDannold N, Sharma S, Hynynen K. Effect of focused ultrasound applied with an ultrasound contrast agent on the tight junctional integrity of the brain microvascular endothelium. Ultrasound Med Biol. 2008; 34:1093–1104. [PubMed: 18378064]
59. Smith DA, Porter TM, Martinez J, Huang S, MacDonald RC, McPherson DD, Holland CK. Destruction thresholds of echogenic liposomes with clinical diagnostic ultrasound. Ultrasound Med Biol. 2007; 33:797–809. [PubMed: 17412486]
60. Taniyama Y, Tachibana K, Hiraoka K, Namba T, Yamasaki K, Hashiya N, Aoki M, Ogihara T, Yasufumi K, Morishita R. Local delivery of plasmid DNA into rat carotid artery using ultrasound. Circulation. 2002; 105:1233–1239. [PubMed: 11889019]

61. Tartis MS, Kruse DE, Zheng H, Zhang H, Kheirolomoom A, Marik J, Ferrara KW. Dynamic microPET imaging of ultrasound contrast agents and lipid delivery. J Control Release. 2008; 131:160–166. [PubMed: 18718854]
62. Unger EC, Hersh E, Vannan M, McCreery T. Gene delivery using ultrasound contrast agents. Echocardiography. 2001; 18:355–361. [PubMed: 11415509]
63. Unger EC, Porter T, Culp W, Labell R, Matsunaga T, Zutshi R. Therapeutic applications of lipid-coated microbubbles. Adv Drug Deliv Rev. 2004; 56:1291–1314. [PubMed: 15109770]
64. Zheng H, Kruse DE, Stephens DN, Ferrara KW, Sutcliffe P, Gardner E. A sensitive ultrasonic imaging method for targeted contrast microbubble detection. Conf Proc IEEE Eng Med Biol Soc. 2008; 2008:5290–5293. [PubMed: 19163911]
65. Lentacker I, Geers B, Demeester J, De Smedt SC, Sanders NN. Design and evaluation of doxorubicin-containing microbubbles for ultrasound-triggered doxorubicin delivery: cytotoxicity and mechanisms involved. Mol Ther. 2010; 18:101–108. [PubMed: 19623162]
66. Lentacker I, Wang N, Vandenbroucke RE, Demeester J, De Smedt SC, Sanders NN. Ultrasound Exposure of Lipoplex Loaded Microbubbles Facilitates Direct Cytoplasmic Entry of the Lipoplexes. Mol Pharm. 2009
67. Deckers R, Yudina A, Cardoit LC, Moonen CT. A fluorescent chromophore TOTO-3 as a 'smart probe' for the assessment of ultrasound-mediated local drug delivery in vivo. Contrast Media Mol Imaging. 2010
68. Eker OF, Quesson B, Rome C, Arsaut J, Deminiere C, Moonen CT, Grenier N, Couillaud F. Combination of cell delivery and thermoinducible transcription for in vivo spatiotemporal control of gene expression: a feasibility study. Radiology. 2011; 258:496–504. [PubMed: 21163917]
69. Hallow DM, Mahajan AD, Prausnitz MR. Ultrasonically targeted delivery into endothelial and smooth muscle cells in ex vivo arteries. J Control Release. 2007; 118:285–293. [PubMed: 17291619]
70. Juffermans LJ, van Dijk A, Jongenelen CA, Drukarch B, Reijerkerk A, de Vries HE, Kamp O, Musters RJ. Ultrasound and microbubble-induced intra- and intercellular bioeffects in primary endothelial cells. Ultrasound Med Biol. 2009; 35:1917–1927. [PubMed: 19766381]
71. Kudo N, Okada K, Yamamoto K. Sonoporation by single-shot pulsed ultrasound with microbubbles adjacent to cells. Biophys J. 2009; 96:4866–4876. [PubMed: 19527645]
72. Meijering BD, Juffermans LJ, van Wamel A, Henning RH, Zuhorn IS, Emmer M, Versteilen AM, Paulus WJ, van Gilst WH, Kooiman K, et al. Ultrasound and microbubble-targeted delivery of macromolecules is regulated by induction of endocytosis and pore formation. Circ Res. 2009; 104:679–687. [PubMed: 19168443]
73. Ohl CD, Arora M, Ikink R, de Jong N, Versluis M, Delius M, Lohse D. Sonoporation from jetting cavitation bubbles. Biophys J. 2006; 91:4285–4295. [PubMed: 16950843]
74. Saito M, Mazda O, Takahashi KA, Arai Y, Kishida T, Shin-Ya M, Inoue A, Tonomura H, Sakao K, Morihara T, et al. Sonoporation mediated transduction of pDNA/siRNA into joint synovium in vivo. J Orthop Res. 2007; 25:1308–1316. [PubMed: 17549706]
75. Tran TA, Le Guennec JY, Bougnoux P, Tranquart F, Bouakaz A. Characterization of cell membrane response to ultrasound activated microbubbles. IEEE Trans Ultrason Ferroelectr Freq Control. 2008; 55:43–49. [PubMed: 18334312]
76. van Wamel A, Kooiman K, Emmer M, ten Cate FJ, Versluis M, de Jong N. Ultrasound microbubble induced endothelial cell permeability. J Control Release. 2006; 116:e100–e102. [PubMed: 17718938]
77. van Wamel A, Kooiman K, Harteveld M, Emmer M, ten Cate FJ, Versluis M, de Jong N. Vibrating microbubbles poking individual cells: drug transfer into cells via sonoporation. J Control Release. 2006; 112:149–155. [PubMed: 16556469]
78. Yudina A, Lepetit-Coiffe M, Moonen CT. Evaluation of the temporal window for drug delivery following ultrasound-mediated membrane permeability enhancement. Mol Imaging Biol. 2011; 13:239–249. [PubMed: 20521134]
79. Chen H, Brayman AA, Bailey MR, Matula TJ. Blood vessel rupture by cavitation. Urol Res. 2010; 38:321–326. [PubMed: 20680255]

80. Chen H, Kreider W, Brayman AA, Bailey MR, Matula TJ. Blood vessel deformations on microsecond time scales by ultrasonic cavitation. Phys Rev Lett. 2011; 106:034301. [PubMed: 21405276]
81. Gaitan DF, Tessien RA, Hiller RA, Gutierrez J, Scott C, Tardif H, Callahan B, Matula TJ, Crum LA, Holt RG, et al. Transient cavitation in high-quality-factor resonators at high static pressures. J Acoust Soc Am. 2010; 127:3456–3465. [PubMed: 20550245]
82. Matula T, Guan J. Using optical scattering to measure properties of ultrasound contrast agent shells. J Acoust Soc Am. 2011; 129:1675.
83. Hernot S, Klibanov AL. Microbubbles in ultrasound-triggered drug and gene delivery. Adv Drug Deliv Rev. 2008; 60:1153–1166. [PubMed: 18486268]
84. Klibanov AL, Shevchenko TI, Raju BI, Seip R, Chin CT. Ultrasound-triggered release of materials entrapped in microbubble-liposome constructs: A tool for targeted drug delivery. J Control Release. 2010
85. Kheirolomoom A, Mahakian LM, Lai CY, Lindfors HA, Seo JW, Paoli EE, Watson KD, Haynam EM, Ingham ES, Xing L, et al. Copper-doxorubicin as a nanoparticle cargo retains efficacy with minimal toxicity. Mol Pharm. 2010; 7:1948–1958. [PubMed: 20925429]
86. Paoli EE, Kruse DE, Seo JW, Zhang H, Kheirolomoom A, Watson KD, Chiu P, Stahlberg H, Ferrara KW. An optical and microPET assessment of thermally-sensitive liposome biodistribution in the Met-1 tumor model: Importance of formulation. J Control Release. 2010; 143:13–22. [PubMed: 20006659]
87. Kheirolomoom A, Kruse DE, Qin S, Watson KE, Lai CY, Young LJ, Cardiff RD, Ferrara KW. Enhanced in vivo bioluminescence imaging using liposomal luciferin delivery system. J Control Release. 2010; 141:128–136. [PubMed: 19748536]
88. Mohan P, Rapoport N. Doxorubicin as a molecular nanotheranostic agent: effect of doxorubicin encapsulation in micelles or nanoemulsions on the ultrasound-mediated intracellular delivery and nuclear trafficking. Mol Pharm. 2010; 7:1959–1973. [PubMed: 20957997]
89. Bohmer MR, Chlon CH, Raju BI, Chin CT, Shevchenko T, Klibanov AL. Focused ultrasound and microbubbles for enhanced extravasation. J Control Release. 2010
90. Bohmer MR, Klibanov AL, Tiemann K, Hall CS, Gruell H, Steinbach OC. Ultrasound triggered image-guided drug delivery. Eur J Radiol. 2009; 70:242–253. [PubMed: 19272727]
91. Chappell JC, Klibanov AL, Price RJ. Ultrasound-microbubble-induced neovascularization in mouse skeletal muscle. Ultrasound Med Biol. 2005; 31:1411–1422. [PubMed: 16223645]
92. Chappell JC, Song J, Burke CW, Klibanov AL, Price RJ. Targeted delivery of nanoparticles bearing fibroblast growth factor-2 by ultrasonic microbubble destruction for therapeutic arteriogenesis. Small. 2008; 4:1769–1777. [PubMed: 18720443]
93. Chappell JC, Song J, Klibanov AL, Price RJ. Ultrasonic microbubble destruction stimulates therapeutic arteriogenesis via the CD18-dependent recruitment of bone marrow-derived cells. Arterioscler Thromb Vasc Biol. 2008; 28:1117–1122. [PubMed: 18403725]
94. Ferrante EA, Pickard JE, Rychak J, Klibanov A, Ley K. Dual targeting improves microbubble contrast agent adhesion to VCAM-1 and P-selectin under flow. J Control Release. 2009; 140:100–107. [PubMed: 19666063]
95. Guenther F, von zur Muhlen C, Ferrante EA, Grundmann S, Bode C, Klibanov AL. An ultrasound contrast agent targeted to P-selectin detects activated platelets at supra-arterial shear flow conditions. Invest Radiol. 2010; 45:586–591. [PubMed: 20808239]
96. Klibanov AL. Preparation of targeted microbubbles: ultrasound contrast agents for molecular imaging. Med Biol Eng Comput. 2009; 47:875–882. [PubMed: 19517153]
97. Patil AV, Rychak JJ, Allen JS, Klibanov AL, Hossack JA. Dual frequency method for simultaneous translation and real-time imaging of ultrasound contrast agents within large blood vessels. Ultrasound Med Biol. 2009; 35:2021–2030. [PubMed: 19828229]
98. Phillips LC, Klibanov AL, Bowles DK, Ragosta M, Hossack JA, Wamhoff BR. Focused in vivo delivery of plasmid DNA to the porcine vascular wall via intravascular ultrasound destruction of microbubbles. J Vasc Res. 2010; 47:270–274. [PubMed: 19923850]

99. Phillips LC, Klibanov AL, Wamhoff BR, Hossack JA. Targeted gene transfection from microbubbles into vascular smooth muscle cells using focused, ultrasound-mediated delivery. Ultrasound Med Biol. 2010; 36:1470–1480. [PubMed: 20800174]

100. Song J, Cottler PS, Klibanov AL, Kaul S, Price RJ. Microvascular remodeling and accelerated hyperemia blood flow restoration in arterially occluded skeletal muscle exposed to ultrasonic microbubble destruction. Am J Physiol Heart Circ Physiol. 2004; 287:H2754–H2761. [PubMed: 15319212]

101. Villanueva FS, Klibanov A, Wagner WR. Microbubble-endothelial cell interactions as a basis for assessing endothelial function. Echocardiography. 2002; 19:427–438. [PubMed: 12174207]

102. Xuan JW, Bygrave M, Valiyeva F, Moussa M, Izawa JI, Bauman GS, Klibanov A, Wang F, Greenberg NM, Fenster A. Molecular targeted enhanced ultrasound imaging of flk1 reveals diagnosis and prognosis potential in a genetically engineered mouse prostate cancer model. Mol Imaging. 2009; 8:209–220. [PubMed: 19728975]

103. Lanza G, Winter P, Cyrus T, Caruthers S, Marsh J, Hughes M, Wickline S. Nanomedicine opportunities in cardiology. Ann N Y Acad Sci. 2006; 1080:451–465. [PubMed: 17132801]

104. Burke CW, Klibanov AL, Sheehan JP, Price RJ. Inhibition of glioma growth by microbubble activation in a subcutaneous model using low duty cycle ultrasound without significant heating. J Neurosurg. 2011

105. Shortencarier MJ, Dayton PA, Bloch SH, Schumann PA, Matsunaga TO, Ferrara KW. A method for radiation-force localized drug delivery using gas-filled lipospheres. IEEE Trans Ultrason Ferroelectr Freq Control. 2004; 51:822–831. [PubMed: 15301001]

106. Tartis MS, McCallan J, Lum AF, LaBell R, Stieger SM, Matsunaga TO, Ferrara KW. Therapeutic effects of paclitaxel-containing ultrasound contrast agents. Ultrasound Med Biol. 2006; 32:1771–1780. [PubMed: 17112963]

107. Soman NR, Marsh JN, Hughes MS, Lanza GM, Wickline SA. Acoustic activation of targeted liquid perfluorocarbon nanoparticles does not compromise endothelial integrity. IEEE Trans Nanobioscience. 2006; 5:69–75. [PubMed: 16805101]

108. Frenkel V, Etherington A, Greene M, Quijano J, Xie J, Hunter F, Dromi S, Li KC. Delivery of liposomal doxorubicin (Doxil) in a breast cancer tumor model: investigation of potential enhancement by pulsed-high intensity focused ultrasound exposure. Acad Radiol. 2006; 13:469–479. [PubMed: 16554227]

109. Frenkel V, Kimmel E, Iger Y. Ultrasound-facilitated transport of silver chloride (AgCl) particles in fish skin. J Control Release. 2000; 68:251–261. [PubMed: 10925133]

110. Frenkel V, Kimmel E, Iger Y. Ultrasound-induced intercellular space widening in fish epidermis. Ultrasound Med Biol. 2000; 26:473–480. [PubMed: 10773379]

111. Hancock H, Dreher MR, Crawford N, Pollock CB, Shih J, Wood BJ, Hunter K, Frenkel V. Evaluation of pulsed high intensity focused ultrasound exposures on metastasis in a murine model. Clin Exp Metastasis. 2009; 26:729–738. [PubMed: 19517258]

112. Hancock HA, Smith LH, Cuesta J, Durrani AK, Angstadt M, Palmeri ML, Kimmel E, Frenkel V. Investigations into pulsed high-intensity focused ultrasound-enhanced delivery: preliminary evidence for a novel mechanism. Ultrasound Med Biol. 2009; 35:1722–1736. [PubMed: 19616368]

113. O'Neill BE, Vo H, Angstadt M, Li KP, Quinn T, Frenkel V. Pulsed high intensity focused ultrasound mediated nanoparticle delivery: mechanisms and efficacy in murine muscle. Ultrasound Med Biol. 2009; 35:416–424. [PubMed: 19081668]

114. Yuh EL, Shulman SG, Mehta SA, Xie J, Chen L, Frenkel V, Bednarski MD, Li KC. Delivery of systemic chemotherapeutic agent to tumors by using focused ultrasound: study in a murine model. Radiology. 2005; 234:431–437. [PubMed: 15671000]

115. Holland CK, McPherson DD. Echogenic Lipsomes for Targeted Drug Delivery. Proc IEEE Int Symp Biomed Imaging. 2009; 2009:755–758. [PubMed: 20383294]

116. Stieger SM, Caskey CF, Adamson RH, Qin S, Curry FR, Wisner ER, Ferrara KW. Enhancement of vascular permeability with low-frequency contrast-enhanced ultrasound in the chorioallantoic membrane model. Radiology. 2007; 243:112–121. [PubMed: 17392250]

117. Lum AF, Borden MA, Dayton PA, Kruse DE, Simon SI, Ferrara KW. Ultrasound radiation force enables targeted deposition of model drug carriers loaded on microbubbles. J Control Release. 2006; 111:128–134. Epub 2005 Dec 2027. [PubMed: 16380187]

118. McDannold NJ, Vykhodtseva NI, Hynynen K. Microbubble contrast agent with focused ultrasound to create brain lesions at low power levels: MR imaging and histologic study in rabbits. Radiology. 2006; 241:95–106. [PubMed: 16990673]

119. Treat LH, McDannold N, Vykhodtseva N, Zhang Y, Tam K, Hynynen K. Targeted delivery of doxorubicin to the rat brain at therapeutic levels using MRI-guided focused ultrasound. Int J Cancer. 2007; 121:901–907. [PubMed: 17437269]

120. Vykhodtseva N, McDannold N, Hynynen K. Induction of apoptosis in vivo in the rabbit brain with focused ultrasound and Optison. Ultrasound Med Biol. 2006; 32:1923–1929. [PubMed: 17169704]

121. Vykhodtseva N, McDannold N, Hynynen K. Progress and problems in the application of focused ultrasound for blood-brain barrier disruption. Ultrasonics. 2008; 48:279–296. Epub 2008 Apr 2014. [PubMed: 18511095]

122. Rapoport N, Kennedy AM, Shea JE, Scaife CL, Nam KH. Ultrasonic nanotherapy of pancreatic cancer: lessons from ultrasound imaging. Mol Pharm. 2010; 7:22–31. [PubMed: 19899813]

123. Rapoport N, Nam K-H, Gupta R, Gao Z, Mohan P, Payne A, Todd N, Liu X, Kim T, Shea J, et al. Ultrasound-mediated tumor imaging and nanotherapy using drug loaded, block copolymer stabilized perfluorocarbon nanoemulsions. J. Control Release. 2011; 153:4–15. [PubMed: 21277919]

124. Rapoport NY, Kennedy AM, Shea JE, Scaife CL, Nam K-H. Controlled and targeted tumor chemotherapy by ultrasound-activated nanoemulsions/microbubbles. J Control Release. 2009; 138:268–276. [PubMed: 19477208]

125. Borden MA, Kruse DE, Caskey CF, Zhao S, Dayton PA, Ferrara KW. Influence of lipid shell physicochemical properties on ultrasound-induced microbubble destruction. IEEE Trans Ultrason Ferroelectr Freq Control. 2005; 52:1992–2002. [PubMed: 16422411]

126. Borden MA, Zhang H, Gillies RJ, Dayton PA, Ferrara KW. A stimulus-responsive contrast agent for ultrasound molecular imaging. Biomaterials. 2008; 29:597–606. [PubMed: 17977595]

127. Gao Z, Fain HD, Rapoport N. Ultrasound-enhanced tumor targeting of polymeric micellar drug carriers. Mol Pharm. 2004; 1:317–330. [PubMed: 15981591]

128. Kheirolomoom A, Dayton PA, Lum AF, Little E, Paoli EE, Zheng H, Ferrara KW. Acoustically-active microbubbles conjugated to liposomes: characterization of a proposed drug delivery vehicle. J Control Release. 2007; 118:275–284. [PubMed: 17300849]

129. Schroeder A, Avnir Y, Weisman S, Najajreh Y, Gabizon A, Talmon Y, Kost J, Barenholz Y. Controlling liposomal drug release with low frequency ultrasound: mechanism and feasibility. Langmuir. 2007; 23:4019–4025. [PubMed: 17319706]

130. Schroeder A, Honen R, Turjeman K, Gabizon A, Kost J, Barenholz Y. Ultrasound triggered release of cisplatin from liposomes in murine tumors. J Control Release. 2009

131. Wheatley MA, Forsberg F, Oum K, Ro R, El-Sherif D. Comparison of in vitro and in vivo acoustic response of a novel 50:50 PLGA contrast agent. Ultrasonics. 2006; 44:360–367. [PubMed: 16730047]

132. Hu Z, Yang XY, Liu Y, Sankin GN, Pua EC, Morse MA, Lyerly HK, Clay TM, Zhong P. Investigation of HIFU-induced anti-tumor immunity in a murine tumor model. J Transl Med. 2007; 5:34. [PubMed: 17625013]

133. Lu P, Zhu XQ, Xu ZL, Zhou Q, Zhang J, Wu F. Increased infiltration of activated tumor-infiltrating lymphocytes after high intensity focused ultrasound ablation of human breast cancer. Surgery. 2009; 145:286–293. Epub 2009 Jan 2025. [PubMed: 19231581]

134. Wu F, Zhou L, Chen WR. Host antitumour immune responses to HIFU ablation. Int J Hyperthermia. 2007; 23:165–171. [PubMed: 17578340]

135. Xing Y, Lu X, Pua EC, Zhong P. The effect of high intensity focused ultrasound treatment on metastases in a murine melanoma model. Biochem Biophys Res Commun. 2008; 375:645–650. Epub 2008 Aug 2024. [PubMed: 18727919]

136. Kripfgans OD, Fowlkes JB, Miller DL, Eldevik OP, Carson PL. Acoustic droplet vaporization for therapeutic and diagnostic applications. Ultrasound Med Biol. 2000; 26:1177–1189. [PubMed: 11053753]
137. Rapoport N, Marin A, Christensen DA. Ultrasound-activated micellar drug delivery. Drug Delivery Syst Sci. 2002; 2:37–46.
138. Rapoport N, Marin A, Luo Y, Prestwich GD, Muniruzzaman MD. Intracellular uptake and trafficking of Pluronic micelles in drug-sensitive and MDR cells: effect on the intracellular drug localization. J Pharm Sci. 2002; 91:157–170. [PubMed: 11782905]
139. Mehier-Humbert S, Yan F, Frinking P, Schneider M, Guy RH, Bettinger T. Ultrasound-mediated gene delivery: influence of contrast agent on transfection. Bioconjug Chem. 2007; 18:652–662. [PubMed: 17419583]
140. Suzuki R, Takizawa T, Negishi Y, Hagisawa K, Tanaka K, Sawamura K, Utoguchi N, Nishioka T, Maruyama K. Gene delivery by combination of novel liposomal bubbles with perfluoropropane and ultrasound. J Control Release. 2007; 117:130–136. [PubMed: 17113176]
141. Ferrara KW, Borden MA, Zhang H. Lipid-shelled vehicles: engineering for ultrasound molecular imaging and drug delivery. Acc Chem Res. 2009; 42:881–892. [PubMed: 19552457]
142. Unger PG. The role of noncontact ultrasound in evidence-based wound care. Director. 2008; 16:14–15. [PubMed: 19343878]
143. Rapoport N, Christensen DA, Kennedy AM, Nam KH. Cavitation properties of block copolymer stabilized phase-shift nanoemulsions used as drug carriers. Ultrasound Med Biol. 2010; 36:419–429. [PubMed: 20133040]
144. Rapoport NY, Efros AL, Christensen DA, Kennedy AM, Nam KH. Microbubble generation in phase-shift nanoemulsions used as anticancer drug carriers. Bub Sci Eng Tech. 2009; 1:31–39.
145. Apfel, RE. Activatable Infusable Dispersions Containing Drops of a Superheated Liquid for Methods of Therapy and Diagnosis. 1998. Vol. 5,840,276
146. Fabiilli ML, Haworth KJ, Fakhri NH, Kripfgans OD, Carson PL, Fowlkes JB. The role of inertial cavitation in acoustic droplet vaporization. IEEE Trans Ultrason Ferroelectr Freq Control. 2009; 56:1006–1017. [PubMed: 19473917]
147. Kripfgans OD, Fabiilli ML, Carson PL, Fowlkes JB. On the acoustic vaporization of micrometer-sized droplets. J Acoust Soc Am. 2004; 116:272–281. [PubMed: 15295987]
148. Kripfgans OD, Fowlkes JB, Woydt M, Eldevik OP, Carson PL. In vivo droplet vaporization for occlusion therapy and phase aberration correction. IEEE Trans Ultrason Ferroelectr Freq Control. 2002; 49:726–738. [PubMed: 12075966]
149. Kripfgans OD, Orifici CM, Carson PL, Ives KA, Eldevik OP, Fowlkes JB. Acoustic droplet vaporization for temporal and spatial control of tissue occlusion: a kidney study. IEEE Trans Ultrason Ferroelectr Freq Control. 2005; 52:1101–1110. [PubMed: 16212249]
150. Lo AH, Kripfgans OD, Carson PL, Fowlkes JB. Spatial control of gas bubbles and their effects on acoustic fields. Ultrasound Med Biol. 2006; 32:95–106. [PubMed: 16364801]
151. Lo AH, Kripfgans OD, Carson PL, Rothman ED, Fowlkes JB. Acoustic droplet vaporization threshold: effects of pulse duration and contrast agent. IEEE Trans Ultrason Ferroelectr Freq Control. 2007; 54:933–946. [PubMed: 17523558]
152. Fabiilli ML, Haworth KJ, Sebastian IE, Kripfgans OD, Carson PL, Fowlkes JB. Delivery of chlorambucil using an acoustically-triggered perfluoropentane emulsion. Ultrasound Med Biol. 2010; 36:1364–1375. [PubMed: 20691925]
153. Fabiilli ML, Lee JA, Kripfgans OD, Carson PL, Fowlkes JB. Delivery of water-soluble drugs using acoustically triggered perfluorocarbon double emulsions. Pharm Res. 2010; 27:2753–2765. [PubMed: 20872050]
154. Zhang M, Fabiilli ML, Haworth KJ, Fowlkes JB, Kripfgans OD, Roberts WW, Ives KA, Carson PL. Initial investigation of acoustic droplet vaporization for occlusion in canine kidney. Ultrasound Med Biol. 2010; 36:1691–1703. [PubMed: 20800939]
155. Miller DL, Kripfgans OD, Fowlkes JB, Carson PL. Cavitation nucleation agents for nonthermal ultrasound therapy. J Acoust Soc Am. 2000; 107:3480–3486. [PubMed: 10875392]

156. Wong Z, Kripfgans OD, Qamar, Fowlkes JB, Bull J. Bubble evolution in acoustic droplet vaporization at physiological temperature via ultra-high speed imaging. Soft Matter. 2011; 7:4009–4011.

157. Miller DL, Song J. Lithotripter shock waves with cavitation nucleation agents produce tumor growth reduction and gene transfer in vivo. Ultrasound Med Biol. 2002; 28:1343–1348. [PubMed: 12467861]

158. Wong Z, Krifgans O, Qamar, Fowlkes J, Bull J. Bubble evolution in acoustic droplet vaporization at physiological temperature via ultra-high speed imaging. Soft Matter. 2011; 7:4009–4016.

159. Barber EJ, Cady GH. Vapor pressures of perfluoropentanes. J Phys Chem. 1956; 60:504–505.

160. Alexandridis P, Holzwarth JF, Hatton TA. Micellization of Poly(ethylene oxide)-Poly(propylene oxide)-Poly(ethylene oxide) Triblock Copolymers in Aqueous Solutions: Thermodynamics of Copolymer Association. Macromolecules. 1994; 27:2414–2425.

161. Caskey CF, Qin S, Dayton PA, Ferrara KW. Microbubble tunneling in gel phantoms. J Acoust Soc Am. 2009; 125:EL183–EL189. [PubMed: 19425620]

162. Caskey CF, Qin S, Ferrara KW. Ultrasound mediated drug delivery: the effect of microbubbles on a gel boundary. Conf Proc IEEE Eng Med Biol Soc. 2009; 2009:134–136. [PubMed: 19965123]

163. Caskey CF, Stieger SM, Qin S, Dayton PA, Ferrara KW. Direct observations of ultrasound microbubble contrast agent interaction with the microvessel wall. J Acoust Soc Am. 2007; 122:1191–1200. [PubMed: 17672665]

164. Kinoshita M, McDannold N, Jolesz FA, Hynynen K. Noninvasive localized delivery of Herceptin to the mouse brain by MRI-guided focused ultrasound-induced blood-brain barrier disruption. Proc Natl Acad Sci U S A. 2006; 103:11719–11723. [PubMed: 16868082]

165. Schad KC, Hynynen K. In vitro characterization of perfluorocarbon droplets for focused ultrasound therapy. Phys Med Biol. 2010; 55:4933–4947. [PubMed: 20693614]

166. Giesecke T, Hynynen K. Ultrasound-mediated cavitation thresholds of liquid perfluorocarbon droplets in vitro. Ultrasound Med Biol. 2003; 29:1359–1365. [PubMed: 14553814]

167. Kawabata K, Yoshizawa A, Asami R. Site-specific contrast imaging with locally induced microbubble from liquid precursors. IEEE Int. Ultrasonic Symp. 2006:517–520.

168. Kawabata K, Sugita N, Yoshikawa H, Azama T, Umemura S. Nanoparticles with multiple perfluorocarbons for controllable ultrasound-induced phase shift. J. Appl. Physics. 2005; 44:4548–4552.

169. Kawabata, K.; Asami, R.; Azuma, T.; Yoshikawa, H.; Umemura, S. IEEE Int. Ultrasonics Symp; 2007. p. 5-8.

170. Cohn CS, Cushing MM. Oxygen therapeutics: perfluorocarbons and blood substitute safety. Crit Care Clin. 2009; 25:399–414. Table of Contents. [PubMed: 19341916]

171. Kaneda MM, Caruthers S, Lanza GM, Wickline SA. Perfluorocarbon nanoemulsions for quantitative molecular imaging and targeted therapeutics. Ann Biomed Eng. 2009; 37:1922–1933. [PubMed: 19184435]

172. Tran TD, Caruthers SD, Hughes M, Marsh JN, Cyrus T, Winter PM, Neubauer AM, Wickline SA, Lanza GM. Clinical applications of perfluorocarbon nanoparticles for molecular imaging and targeted therapeutics. Int J Nanomedicine. 2007; 2:515–526. [PubMed: 18203420]

173. Winter PM, Cai K, Caruthers SD, Wickline SA, Lanza GM. Emerging nanomedicine opportunities with perfluorocarbon nanoparticles. Expert Rev Med Devices. 2007; 4:137–145. [PubMed: 17359221]

174. Caruthers SD, Cyrus T, Winter PM, Wickline SA, Lanza GM. Anti-angiogenic perfluorocarbon nanoparticles for diagnosis and treatment of atherosclerosis. Wiley Interdiscip Rev Nanomed Nanobiotechnol. 2009; 1:311–323. [PubMed: 20049799]

175. Wickline SA, Neubauer AM, Winter PM, Caruthers SD, Lanza GM. Molecular imaging and therapy of atherosclerosis with targeted nanoparticles. J Magn Reson Imaging. 2007; 25:667–680. [PubMed: 17347992]

176. Wilson K, Homan K, Emelianov S. Biomedical photoacoustics beyond thermal expansion using triggered nanodroplet vaporization for contrast-enhanced imaging. Nat Commun. 2012; 3:618. [PubMed: 22233628]

177. Sheeran PS, Luois S, Dayton PA, Matsunaga TO. Formulation and acoustic studies of a new phase-shift agent for diagnostic and therapeutic ultrasound. Langmuir. 2011; 27:10412–10420. [PubMed: 21744860]

178. Reznik N, Williams R, Burns PN. Investigation of vaporized submicron perfluorocarbon droplets as an ultrasound contrast agent. Ultrasound Med Biol. 2011; 37:1271–1279. [PubMed: 21723449]

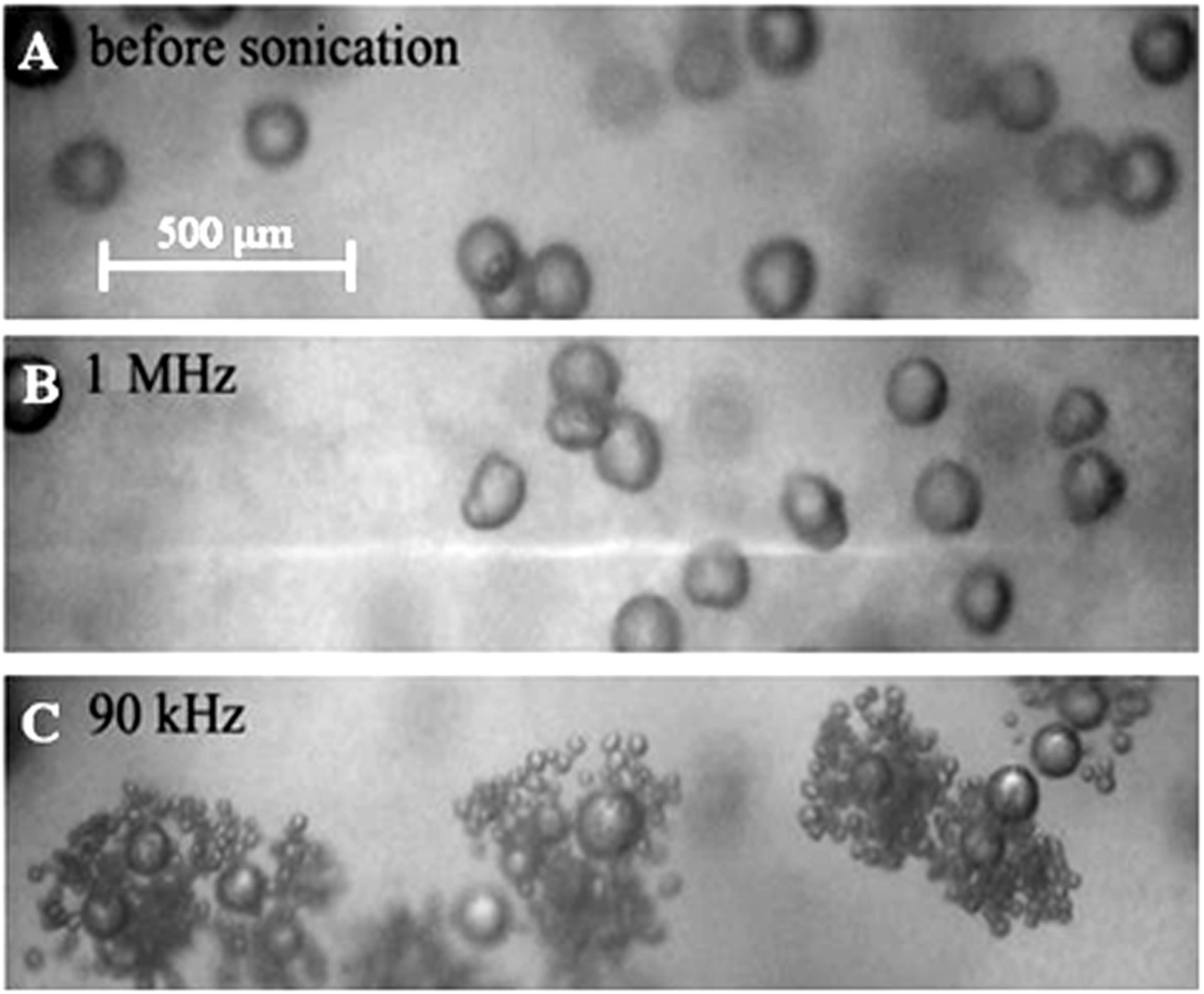

Figure 1.
DDFP/PEG-PLLA microbubbles inserted into a plasma clot (A) – before; (B) and (C) - after 1-min sonication at room temperature; ultrasound parameters: (B) – 1 MHz, 3.4 W/cm2 nominal power density; (C) – 90 kHz, 2.8 W/cm^2.

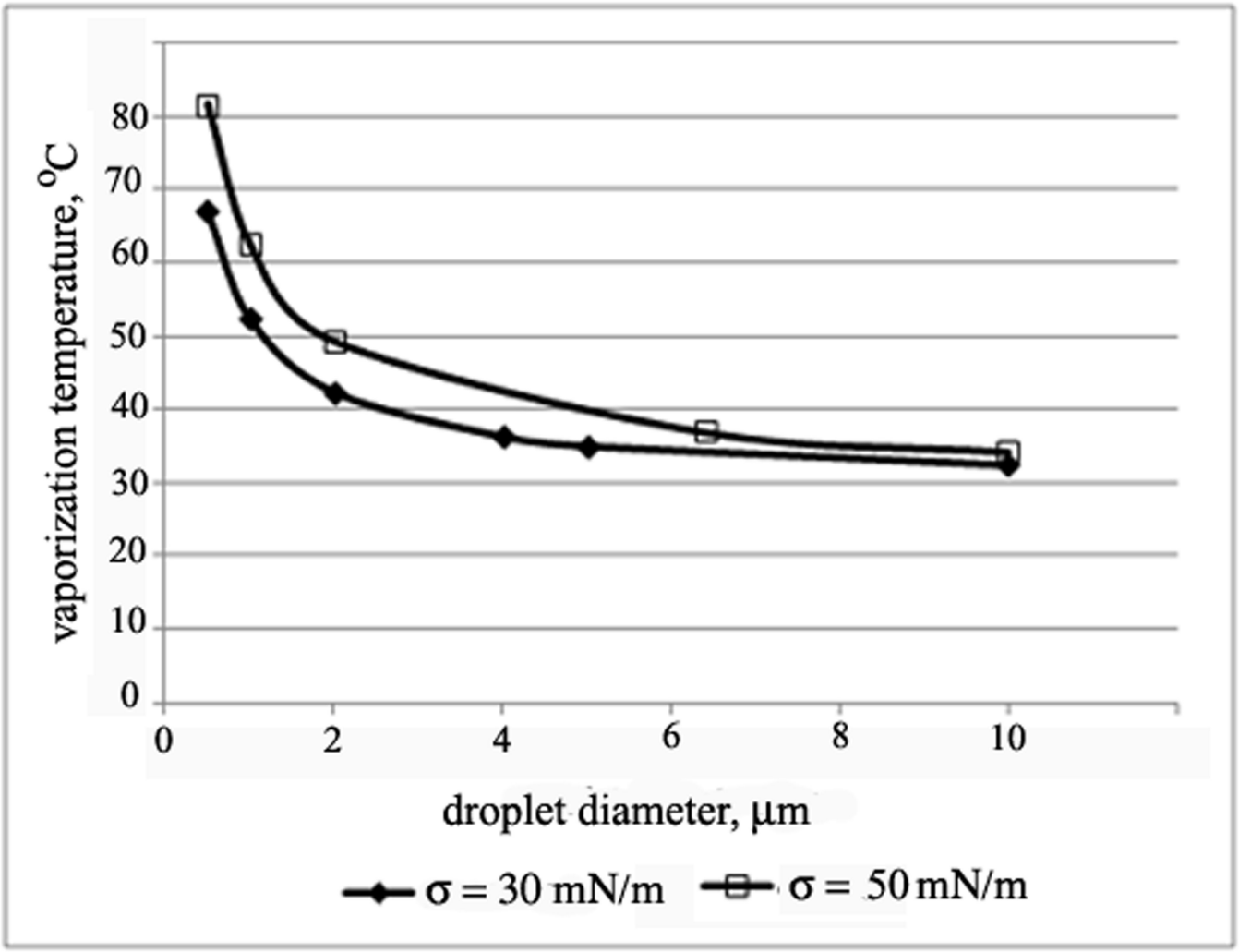

Figure 2.
Calculated dependence of the DDFP vaporization temperature on the droplet size for two values of the surface tension, 30 mN/m and 50 mN/m.

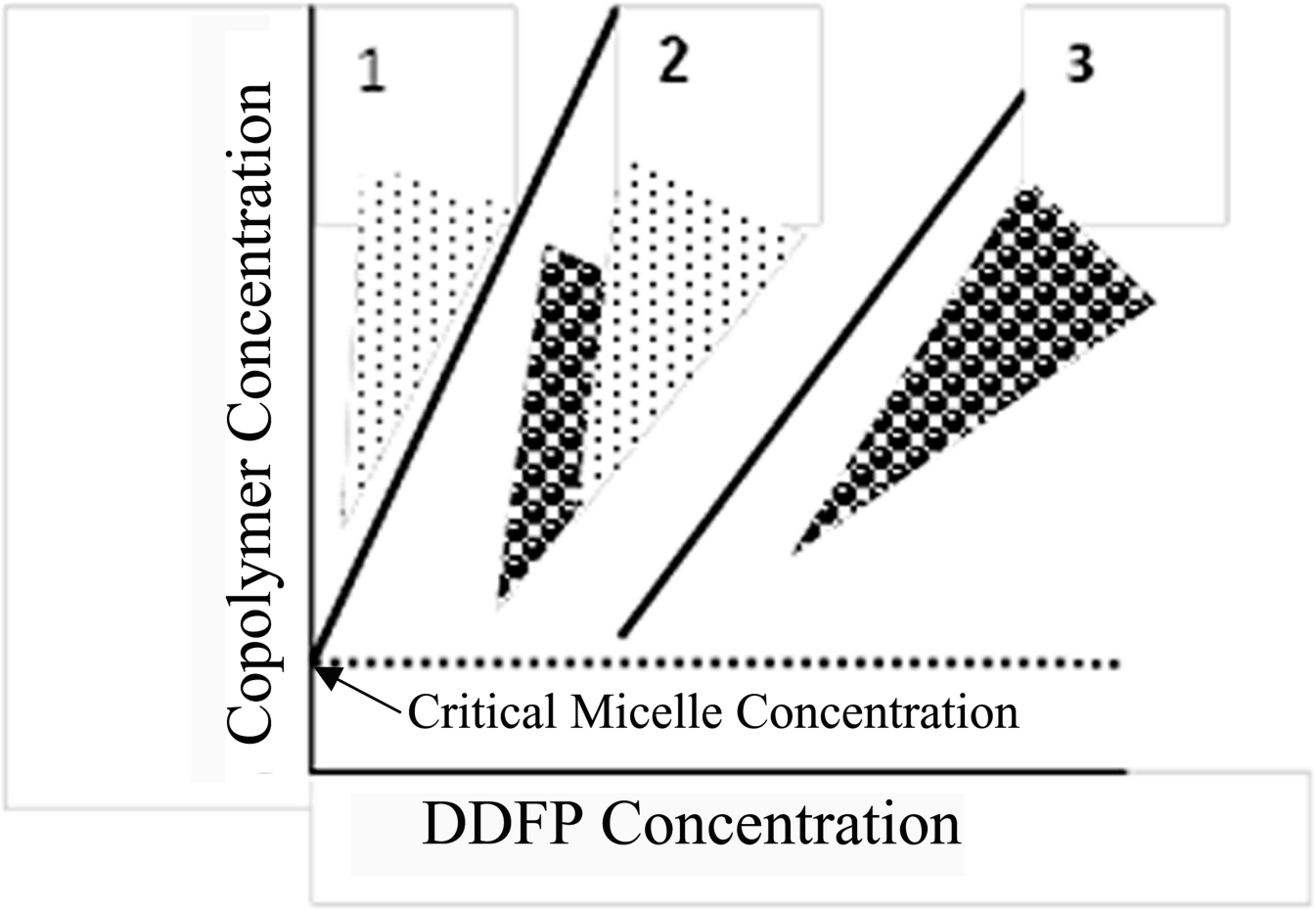

Figure 3.
Schematic representation of the phase diagram of PFC/copolymer formulation in aqueous environment: points – micelles; circles – droplets. The dotted line corresponds to critical micelle concentration of copolymer below which neither micelles nor droplets can be formed. Zone 1 corresponds to micellar solutions with PFC dissolved in micelle cores; zone 2 corresponds to micelle/droplet mixtures; finally, zone 3 corresponds to droplets only. At a fixed copolymer concentration, transition proceeds from zone 1 to zone 2 to zone 3 upon increasing PFC concentration. Adapted from ref. [56] with permission.

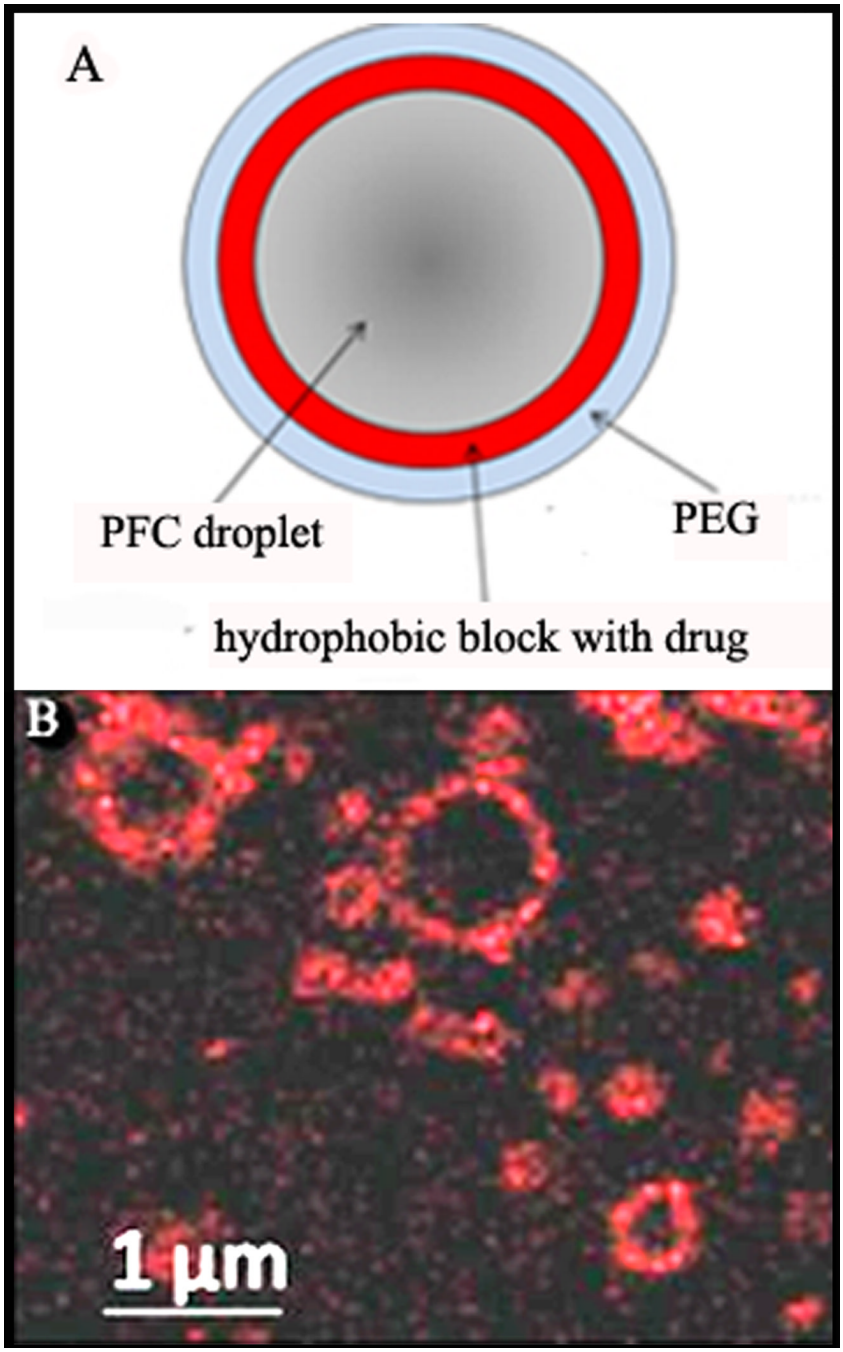

Figure 4.

(A) – The scheme of the nanodroplet structure. In nanodroplets, perfluorocarbon compounds form droplet cores while amphiphilic block copolymers form droplet shells that contain two layers. The inner layer is formed by the hydrophobic block of the block copolymer (e.g. polylactide or polycaprolactone) while the outer layer is formed by the hydrophilic block, PEG. Lipophilic drugs are encapsulated in the hydrophobic inner layer. (B) - laser confocal images of the PFCE/PEG-PCL droplets with encapsulated DOX. Some micrometer-scale droplets presented in panel (B) have been specially generated for better visualization of DOX distribution. DOX localization on the droplet surface is manifested by fluorescence.

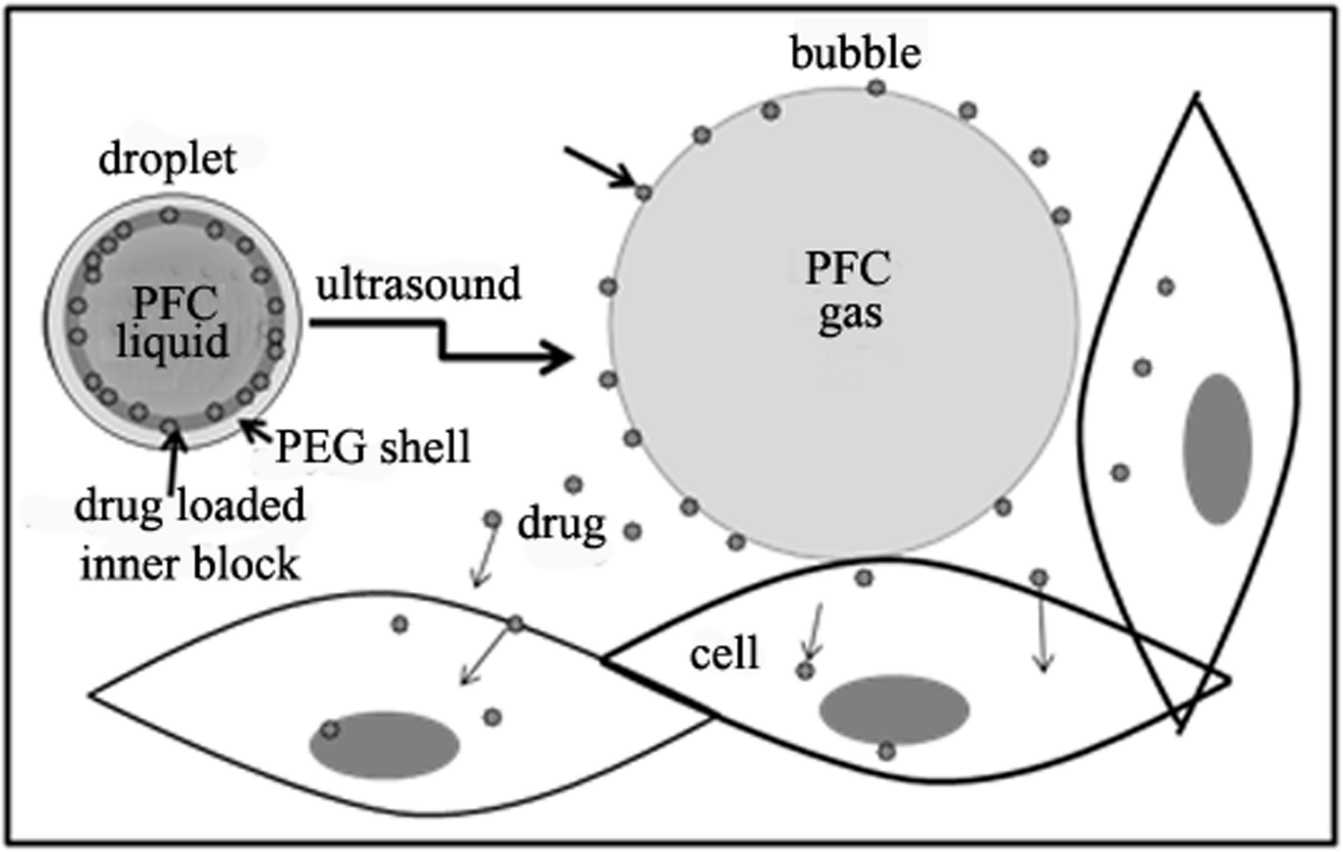

Figure 5.
Schematic illustration of drug transfer from droplets to bubbles to cells under the action of ultrasound. Adapted from ref. [124] with permission from Elsevier.

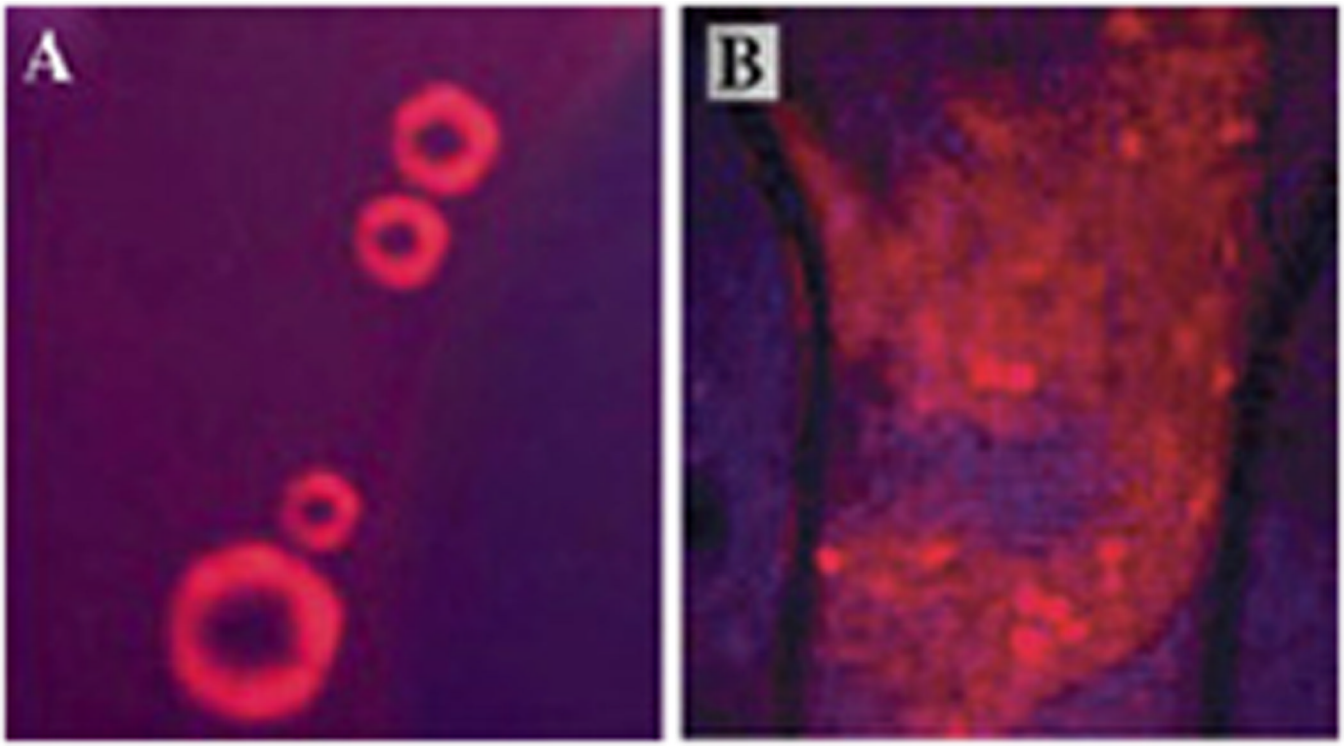

Figure 6.
(A) - The doxorubicin-derived fluorescence (red) of the microbubbles was clearly localized in the bubble walls formed by the bubble-stabilizing copolymer. (B) – upon a 30-s exposure to 3-MHz ultrasound at 2 W/cm^2 power density, the cells incubated with DOX-loaded microbubbles acquired strong fluorescence while bubbles lost fluorescence or were popped. Modified from ref. [56].

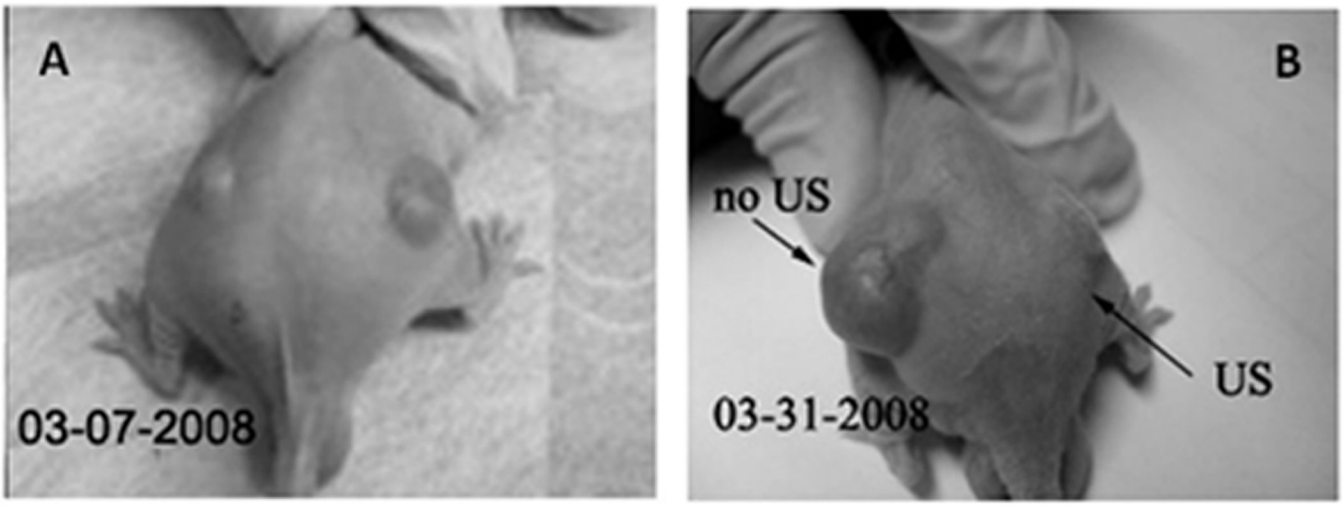

Figure 7.

A mouse bearing bi-lateral ovarian carcinoma tumors was treated by four systemic injections of nanodroplet encapsulated PTX (20 mg/kg as PTX) given twice weekly; only one (the right) tumor was sonicated by1-MHz ultrasound at a nominal output power density 3.4 W/cm2, exposure duration 1 min; ultrasound was delivered 4.5 hours after the injection of the drug formulation. The left tumor grew at the same rate as untreated controls tumors while the right tumor appeared completely resolved. Adapted from ref. [124] with permission from Elsevier.

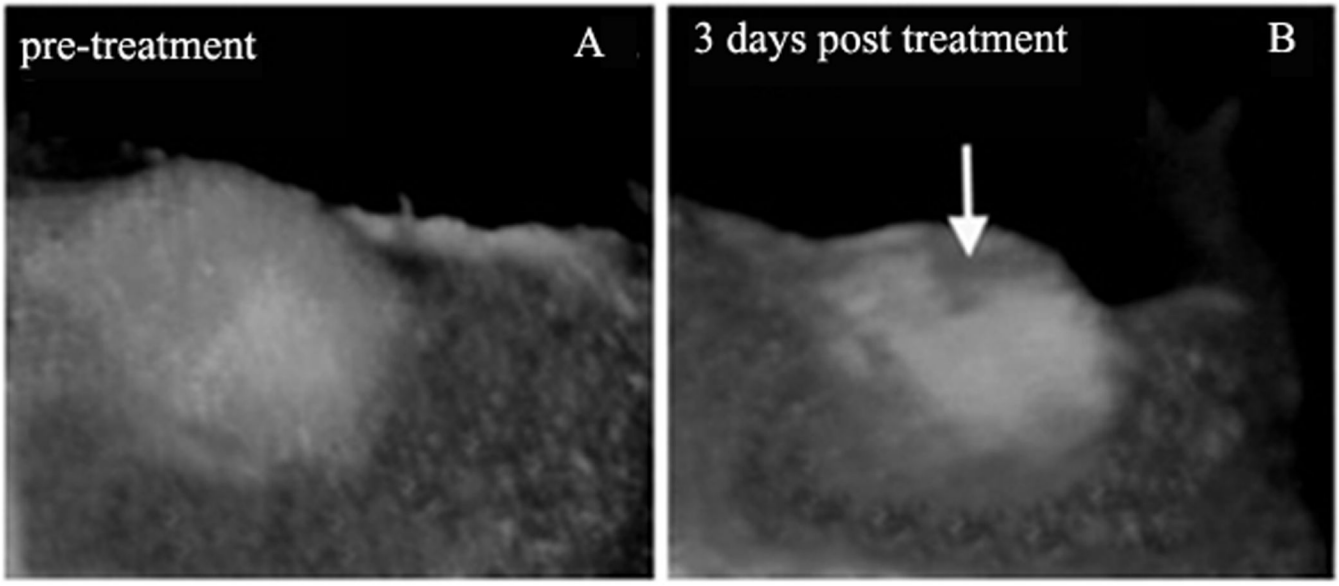

Figure 8.
Intravital fluorescence images of subcutaneous pancreatic tumors before (A) and 3 days after focused ultrasound treatment (B). A mouse was injected with PTX-loaded droplets 1% PFCE/5%PEG-PDLA droplets six hours before ultrasound treatment; DOX dose was 40 mg/kg. Conditions of ultrasound treatment: Ultrasound beam was steered for 50 s in a circle of 4 mm diameter (8 “points”, 200 ms/point, 30 circles per treatment resulting in a total 6 s sonication of each “point” with a maximum power density in the focal zone of 54 W/cm2). MRI thermometry showed tumor heating by about 10 °C. Adapted from ref. [123] with permission from Elsevier.

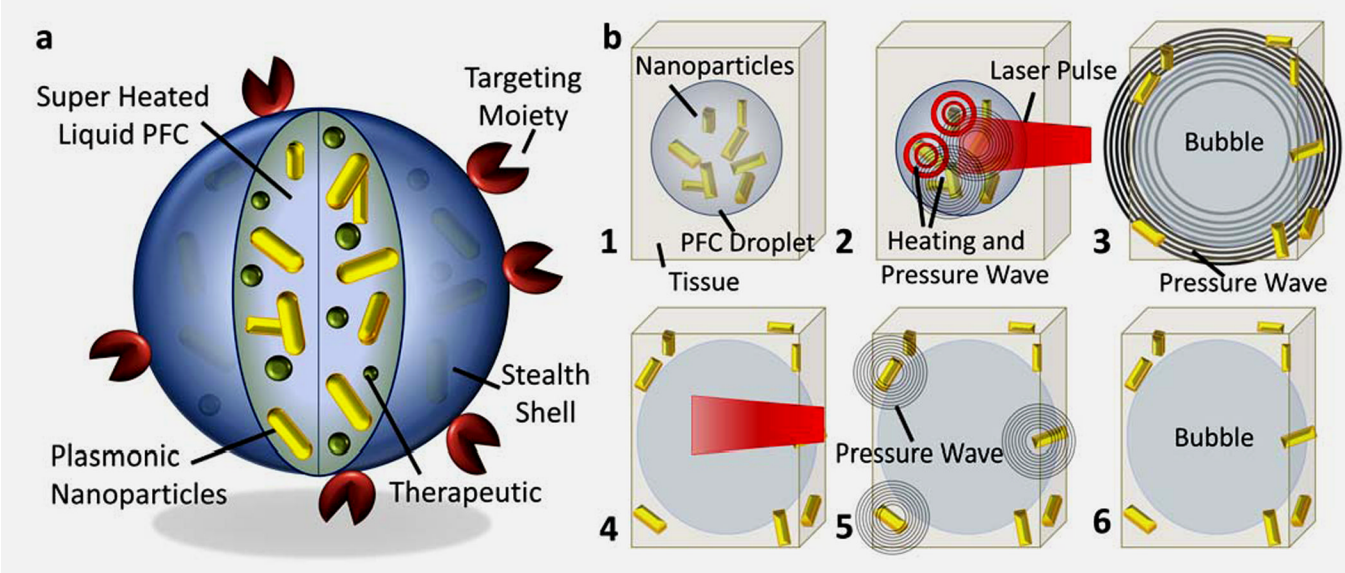

Figure 9.

Photoacoustic nanodroplets (PAnD) concept and mechanisms. (a) Diagram depicting the dual-contrast agent concept – photoacoustic droplet consisting of plasmonic nanoparticles suspended in encapsulated PFC (a super-heated liquid at body temperature) and capped with a BSA shell. PAnDs may further contain therapeutic cargo and be surface functionalized for molecular targeting and cell-particle interactions. (b) Step-by-step diagram of remote activation of PAnDs, providing photoacoustic signal via two mechanisms: vaporization of PAnDs (steps 2–3) and thermal expansion caused by plasmonic nanoparticles (steps 4–5). The resulting gas microbubble of PFC (step 6) provides ultrasound contrast due to acoustic impedance mismatch between gas and the surround environment. Adapted from ref.[176] with permission.

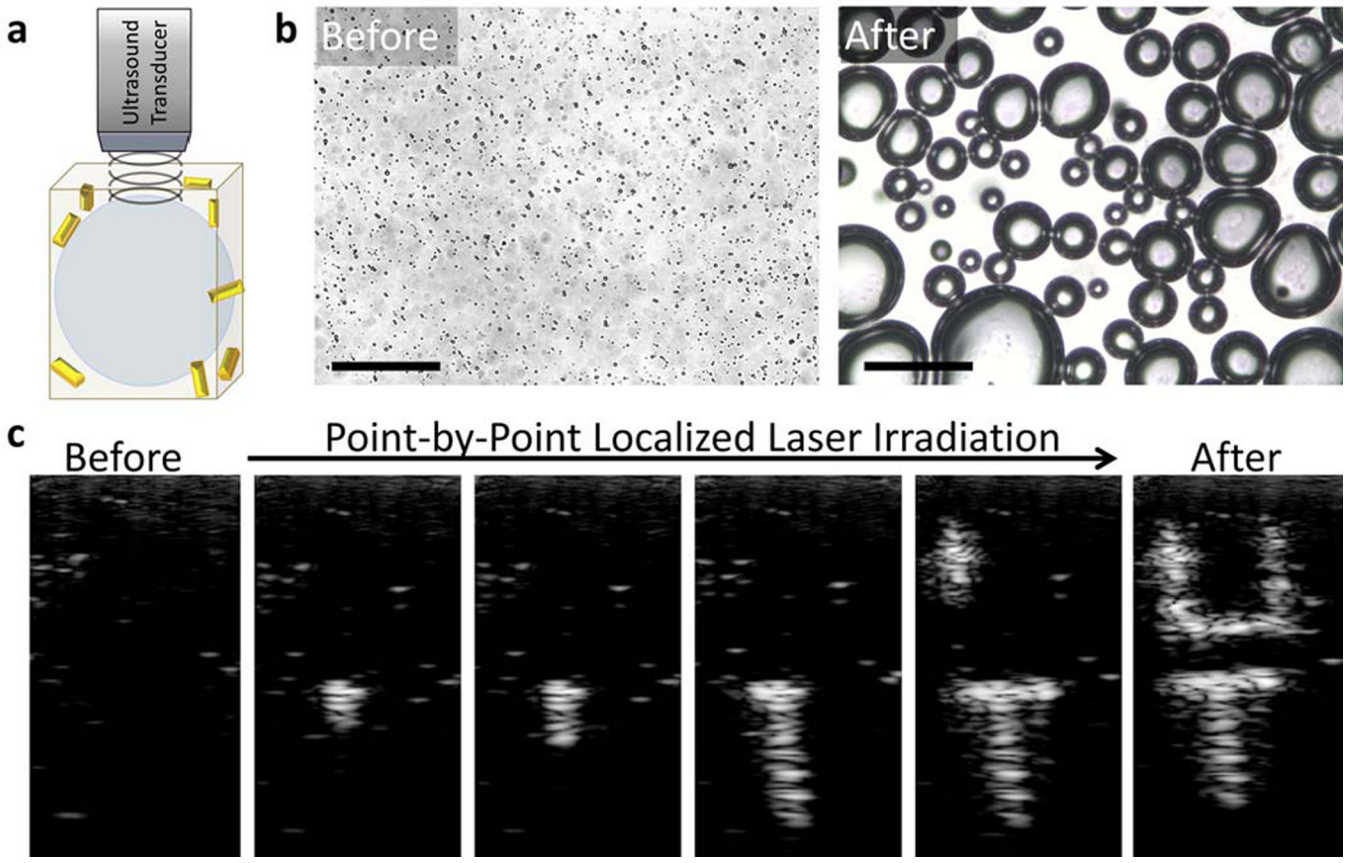

Figure 10.

Ultrasound contrast enhancement *in vitro*. (a) Depiction of the gas phase of a PAnD after laser triggered vaporization has occurred. These microbubbles provide significant acoustic impedance mismatch between the PFC gas and the surrounding environment. (b) Optical images of a hydrogel with PAnDs before laser exposure and after laser exposure. Individual droplets are expected to create bubbles approximately 5 time the diameter of the original droplet. The larger bubbles are due to rapid coalescence of smaller bubbles. Scale bars represent 50 μm. (c) Sequential US frames captured as the laser irradiation produced desired pattern in the phantom. The image before laser irradiation illustrates that the ultrasound field alone does not activate PAnDs (i.e., does not initiate the liquid-to-gas transfer of the PFC). As PAnDs are irradiated with laser beam at corresponding positions, the microbubbles are locally triggered, resulting in ultrasound contrast enhancement. Each individual spot is approximately 1 mm, with the final letters standing 1.2 cm tall and 0.5 cm wide. Images are in 20 dB scale. Adapted from ref.[176] with permission.

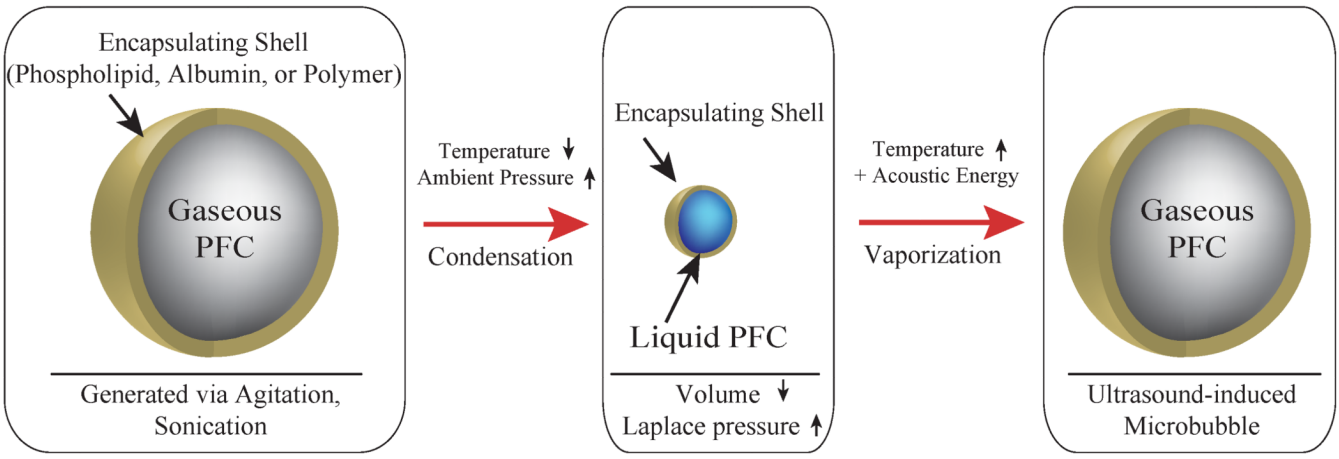

Figure 11.
Schematic representation of the generation of lipid-encapsulated decafluorobutane (DFB) nanodroplets based upon condensation of preformed DFB microbubbles. Adapted from ref.[177] with permission.